machines

MDPI

Article

Design and Optimization of an Additively Manufactured Two-DOF Tuned Mass Damper for Chatter Stability in Boring Process

Saravanamurugan Sundaram [1], Shravan Chidambaresh [1], Krishna Prakash Jayaprakash [1], Jana Petru [2,*] and Thenarasu Mohanavelu [1,*]

[1] Department of Mechanical Engineering, Amrita School of Engineering, Coimbatore, Amrita Vishwa Vidyapeetham, Coimbatore 641112, India
[2] Department of Machining, Assembly and Engineering Metrology, Faculty of Mechanical Engineering, VSB-Technical University of Ostrava, 70800 Ostrava, Czech Republic
* Correspondence: jana.petru@vsb.cz (J.P.); m_thenarasu@cb.amrita.edu (T.M.)

Abstract

Passive tuned mass dampers (TMDs) can reduce chatter, but designing and fabricating an accurately tuned absorber remains challenging due to manufacturing constraints. This study proposes a Design of Experiments and Finite Element Analysis (DOE-FEA) based constrained design optimization framework for a passive two-degree-of-freedom (TDOF) TMD to suppress regenerative chatter in boring operations by considering practical and manufacturing constraints on absorber position, mass ratio, moment of inertia and fixed inter-spring distance. The proposed, additively manufactured TMD housing, made from polylactic acid (PLA), includes a mass block supported by two spring-damper elements that enable coupled translational and rotational interactions with the boring bar. A finite-element forced vibration analysis of the boring bar TMD system is developed to obtain the real and imaginary parts of the frequency response function (FRF), which are then used to construct the stability lobes. The minimum limiting depth of cut over the spindle speed range is used as the optimization criterion, and response surface methodology (RSM) is used to obtain optimum absorber parameters within realistic design constraints. The dynamic behaviour of the TDOF TMD is experimentally and numerically evaluated and compared with that of a single-degree-of-freedom (SDOF) TMD, attributing the relative improvement in performance primarily to the combined effects of independent absorber architecture, mass, stiffness and damping distribution and dynamic tuning. The results showed that the optimal TDOF TMD achieved a DOC of 11.054 mm, while the SDOF TMD achieved 4.335 mm. The experimental investigation of additively manufactured TDOF and SDOF TMDs demonstrated qualitatively similar dynamic phenomena to those of the corresponding numerically optimized absorbers. Time-domain acceleration response, spectrogram and power spectrum were used to compare these dynamic phenomena demonstrated by the SDOF and TDOF TMDs. A reduction in corresponding first and second amplitude peaks from −2.8 dB (670 Hz) and −22.7 dB (1360 Hz) in the case of the SDOF TMD to −17.6 dB (600 Hz) and −23.8 dB (1150 Hz) for the TDOF TMD verified the vibration attenuation and frequency redistribution phenomenon as exhibited by the FE-model.

Keywords: regenerative chatter; boring process; stability lobe; tuned mass dampers; additive manufacturing; polylactic acid

Check for updates

Academic Editors: Diego Ledezma-Ramirez, Pablo Ernesto Tapia-González and César M. A. Vasques

Received: 27 June 2026
Revised: 14 August 2026
Accepted: 20 August 2026
Published: 28 August 2026

Copyright: © 2026 by the authors. Licensee MDPI, Basel, Switzerland. This article is an open access article distributed under the terms and conditions of the Creative Commons Attribution (CC BY) license.

1. Introduction

Machining vibrations generated due to dynamic interactions between cutting tool and workpieces significantly affect machining performance, dimensional accuracy of the parts and surface integrity. These vibrations can be categorized as free vibrations, forced vibrations and self-created vibrations, where the latter is often called chatter. It is an undesirable phenomenon that can cause unstable cutting oscillations, poor surface quality, slower material removal rate, premature tool wear, high noise levels and higher energy consumption due to the dynamic cutting forces acting on the tool-workpiece system exceeding its structural stiffness [1]. At the same time, the cantilevered structure and the large slenderness ratio of the boring bar in boring operation further aggravates the problem, resulting in a significant decrease in the transverse stiffness, making the boring bar susceptible to dynamic instability [2].

Tuned mass dampers (TMDs) have proven to be an effective and practical solution among the different available chatter suppression methods because of their tuneability and versatility. In the passive case, TMDs achieve vibration suppression through proper tuning of the absorber mass, stiffness and damping near the dominant structural modes, while in the active case, the TMDs utilize externally controlled feedback mechanisms for adaptive vibration suppression. While active damping systems provide more flexibility, they are typically more expensive, complex to control, and difficult to design for industrial applications [3,4]. For practical applications, passive absorbers are therefore a preferred option, especially in the machining process.

The vibration absorber-based chatter suppression technique has been widely studied in the field of machine tool chatter suppression. Sims had previously developed the absorber tuning principles for chatter suppression for machining and Yang et al. applied this concept by optimization of a 2-DOF passive vibration absorber combining both translational and rotational modes [5,6]. Wang et al. suggested an embedded passive TMD in a hollow cutting tool and demonstrated that the chatter stability can be enhanced by optimizing analytical tuning parameters of the TDOF TMD based on a continuous beam model with an embedded TDOF absorber. An approach that requires solving the coupled dynamic equations through multiple iterations and finally converting the optimized parameters into physically meaningful properties of spring and damper. Moreover embedding the absorber inside the boring tool is only possible through a machined cavity, that introduces geometric inconsistencies, severely altering the structural stiffness, increasing manufacturing complexity [7]. For slender milling tools, Ma et al. explored passive absorbers mounted to the arbor, and for the case of resonant vibrations, Burattini et al. demonstrated the effectiveness of added inertia through experiments [8,9]. Other approaches such as adaptive and semi-active chatter control have also been investigated, including variable-mass tuning mechanisms and actively controlled damping systems [10]. The passive absorber workpiece-mounted strategies have also proven to be effective in thin-walled machining applications [11,12].

Similarly, a number of configurations of chatter suppressing absorbers have been studied for boring operations. Using magnetorheological fluids, Piezoelectric driven, Variable parameter, Electrorheological fluid damped boring bars passive dynamic vibration absorbers, constrained viscoelastic damping, and tuned particle dampers, measurable improvements have been shown in chatter stability [13–16]. Specific damping solutions for short diameter boring bars and deep hole boring have also been suggested [17,18]. Real-time frequency response measurement (RFRM) based automatic tuning mechanisms have exhibited a higher level of adaptability in the field of boring chatter suppression [19]. Boring bars have also been the subject of research involving the concepts of internal friction damping and inverse cantilever damping [20,21]. The importance of the relation-

ship between chatter stability and absorber parameters (such as absorber mass, stiffness and damping) and position of the absorber on the tool was also highlighted in foundational studies [22,23]. Advanced control strategies like state-filtered rejection schemes, employing an active feedback control approach streamlined for systems exhibiting nonlinear behaviour with matched and mismatched disturbances use state filtering, disturbance estimation and command filtered backstepping to actively support uncertainty and abrupt disturbances [24]. Actor-critic-based neuroadaptive reinforcement learning is implemented to solve high-dimensional uncertainty in nonlinear systems with the system dynamics approximated by a multilayer neural network and an extended state observer to external disturbances [25,26].

A recent study implementing finite element (FE) methods to predict chatter has pointed to the necessity of realistic structural dynamic representation to make accurate chatter stability evaluation by presenting a finite element-based digital twin framework, combining numerical and analytical stability analysis, to predict boring stability [27]. Nevertheless, most of the current studies are still based on simplified lumped-parameter analytical models and empirical tuning expressions, or unconstrained optimization methods which may not account for realistic constraints of absorber design. In addition, internally integrated absorber systems have practical limits in terms of manufacturability, maintenance and retrofitting for commercial use.

Additive manufacturing presents new opportunities for customized vibration absorber development due to geometric flexibility, rapid fabrication capability, and material tunability. PLA is a polymeric material which has inherent damping properties and offers a lightweight structure and flexibility of the absorber. Recent research has shown the vibration attenuation ability of additively manufactured polymer damping structures like polymer pads, embedded damping architectures, and bio-inspired viscoelastic damping systems [28–31]. It has also been reported that damping properties of polymer-based additively manufactured structures are temperature-dependent [32]. Based on the reviewed literature, the use of externally mounted additively manufactured passive tuned mass dampers for chatter suppression in boring, however, has been studied on a limited scale.

To address these challenges, the present study introduces a hybrid finite element–analytical approach for passive tuned mass damper control of chatter in boring operations by altering the dynamic behaviour of the tool. The chatter behaviour and the frequency response characteristics of the tool tip are simulated in ANSYS Mechanical APDL by modelling the boring bar–absorber system to obtain realistic structural dynamic and chatter stability analysis in accordance with Altintas' frequency domain stability criterion [33]. A systematic approach for the optimization of absorber parameters is used by employing a response surface methodology (RSM) framework, which enables to incorporate practical manufacturing constraints. The novelty of the proposed methodology lies in how a FE-prediction model of the boring bar frequency response is coupled with a constrained parametric optimization with respect to the TMD geometry—used to passively tune the TMD parameters without the active online computation or external actuation by providing a simple, autonomous and manufacturable solution. In this light, the use of advanced strategies like disturbance-rejection and neuroadaptive control could best be employed to complement rather than substitute the proposed hybrid constrained optimization approach and pairing the two approaches into a hybrid-active-passive chatter mitigation framework could be a promising prospect to explore in the future.

In addition, this work introduces an externally mounted additively manufactured passive absorber architecture made with PLA material to enable flexible design possibilities for absorber parameters (mass, stiffness and damping characteristics), while offering ease of fabrication and implementation. A comparative study of single-degree-of-freedom (SDOF)

and two-degree-of-freedom (TDOF) additively manufactured passive tuned mass dampers was conducted through experimental validation using time-domain acceleration, power spectrum, and spectrogram analysis. The experiments aimed to examine whether the additively manufactured absorbers exhibited the comparative qualitative dynamic behaviour predicted by the hybrid FEA-RSM numerical optimisation framework, in the form of vibration attenuation and frequency redistribution of the primary system's dominant chatter mode. In the current work, the experimental study serves as a proof-of-concept assessment of the externally mounted additively manufactured TMD rather than a quantitative validation of the optimum stability limit of the TDOF TMD obtained through the numerical optimisation framework. The proposed approach combines realistic structural modelling and system optimisation while integrating manufacturability constraints, establishing an effective framework for chatter suppression in boring applications.

The remainder of this paper is organised as follows. Section 2 discusses the methodology involved in the design and fabrication of various components of the TMD. The theoretical aspects associated with the proposed methodology have been discussed in Section 3, and the Numerical model and the use of RSM to optimise the proposed TDOF TMD have been elaborated in Section 4. The experimental setup employed to carry out the boring operation is described in Section 5. The interpretation of the results and observations obtained through experimental validation of the SDOF and TDOF TMD system is provided in Section 6. This is then followed by a discussion of the scope of the proposed design in various fields of application in Section 7. Finally, the manuscript is concluded by summarising the proposed methodology while also highlighting future scope for development and improvement of the proposed ideas in Section 8.

2. Methodology Selection and Fabrication

The feasibility for implementation of the TMD in boring applications is realized through material selection, a practical design and a suitable method for fabrication. This section discusses PLA as a suitable material choice, Fused Deposition Modelling (FDM) as an appropriate means for fabrication while also highlighting various design aspects associated with the TMD and its spring-mass elements.

2.1. Material Selection and Fabrication

PLA was selected to fabricate the TMD frame because it can be used to manufacture complex geometries, maintains stable dimensions, is lightweight, and has good damping properties. Compared with traditional thermoplastics like ABS, PLA offers advantages such as better stiffness, processability, and dimensional accuracy, which are crucial for customised external-mounted absorber geometries [34–37]. The TMD frame was fabricated using a conventional method called fused deposition modelling (FDM). The FDM approach was chosen for its cost, rapid prototyping capability, and flexibility in creating customised geometries needed to implement the absorber design. Additive manufacturing also allows for quick design changes and practical tuning of absorber configurations for various boring bar geometries. FDM was carried out using eSUN 1.75 mm PLA filament (Shenzhen Esun Industrial Co., Ltd., Shenzhen, China) on a SPAAR3D-LAPWING V1 3D printer (SPAAR3D, Coimbatore, India). UltiMaker Cura slicing software (version 5.3.0; Ultimaker B.V., Zaltbommel, The Netherlands) was used to convert the digital models into G-codes. Table 1 lists the FDM printing parameters used to fabricate the TMDs.

The Elastic modulus 'EXY', reported in Table 1, corresponds to the Young's modulus of 3D-printed PLA along the XY direction (in-plane direction), with loading primarily considered to be parallel to the deposited layer, as is relevant in the current work. 3D-printed components generally exhibit directional mechanical properties, and these properties can

change with raster angle. Hence, 'Modulus orientation' is specified explicitly based on the build and infill orientation. The in-plane Young's Modulus of PLA is used for fabrication of the physical TMD components and is provided solely to enable characterization and reproducibility of the absorber frame.

Table 1. FDM printing parameters for fabricated TMDs.

Parameter	Value
Infill density	50%
Layer thickness	0.07 mm
Layer stacking direction	Z direction
Nozzle diameter	0.4 mm
Nozzle temperature	195 °C
Bed temperature	60 °C
Printing speed	40 mm/s
Infill pattern	Offset grid (45°)
Coordinate alignment	XY plane (load direction)
Raster angle	0°
Build orientation	Flat
Wall and top/bottom layer count	2
Effective Elastic Modulus E_{XY}	1.5 GPa
Modulus orientation	In-plane
Structural damping ratio	0.05

2.2. Design of Tuned Mass Dampers

The TMDs were designed based on geometry and dimensions of the boring bar. They were designed in such a way that the boring bar could be inserted into the 3D-printed TMD frame made of PLA. PLA was used to fabricate the TMD frame as it was observed to have damping properties as mentioned in Table 1. The TMD frame has been provided with space to mount a spring-mass setup with adequate clearance for oscillation. Figure 1 represents the part drawing of the proposed TDOF TMD model.

The proposed design of the TMD offers versatility with respect to its tuneability. The external-mounting design of absorber frame, provided with an internal cavity to mount a spring-mass setup serves as an effective and simple means of altering the stiffness and mass. The dimensions of the cavities within the absorber frame were determined based on geometrical requirements, of the spring-mass setup which were obtained as pre-constraints directly dependent on the design requirements of stiffness and mass elements of the absorber. The dimensions of the vertical cavities to house springs were determined based on the outer diameter of the spring while the dimensions of the horizontal cavity accommodating the cylindrical absorber mass were ascertained based on dimensions of the cylindrical mass along with radial clearance to prevent contact during its oscillatory motion. The length of the horizontal cavity was determined based on mass-block length, inter-spring spacing (30 mm) and the arrangement of spring supports and assembly allowances considering the space occupied by the floating piece and bottom seal. Consequently, this tailor-made cavity was shaped by geometric constraints influenced by the internal architecture of the TMD and associated relative motion ensuring strict confinement of the movement of the spring-mass unit along the direction of primary translational and rotational modes.

The proposed TMD design offers versatility through its tuneability. The external-mounting design of the absorber frame, with an internal cavity for mounting a spring-mass setup, provides an effective, simple way to adjust stiffness and mass. The cavity dimensions within the absorber frame were determined based on the geometrical requirements of the spring-mass setup, which were obtained as pre-constraints directly dependent on the

design requirements of the absorber's stiffness and mass elements. The dimensions of the vertical cavities to house the springs were determined based on the spring's outer diameter, while the dimensions of the horizontal cavity accommodating the cylindrical absorber mass were ascertained based on the mass's dimensions, along with radial clearance to prevent contact during oscillatory motion. The length of the horizontal cavity was determined based on the mass-block length, inter-spring spacing (30 mm), and the arrangement of spring supports and assembly allowances, considering the space occupied by the floating piece and bottom seal. Consequently, this tailor-made cavity was shaped by geometric constraints influenced by the internal architecture of the TMD and associated relative motion, ensuring strict confinement of the spring-mass unit's movement along the primary translational and rotational modes.

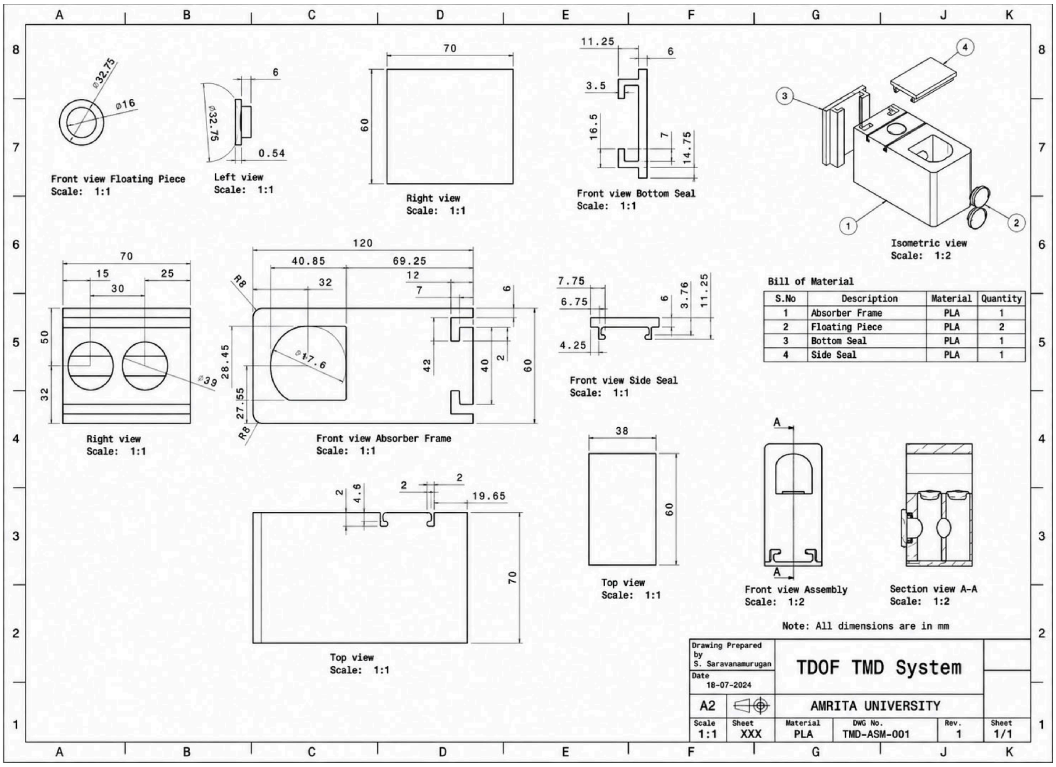


Figure 1. Part drawing of TDOF TMD.

The spring-mass setup is held in position between the floating piece and bottom seal. While the mass rests between the springs, the bottom seal supports and holds the bottom springs in compression. The top springs, placed directly under the vibrating main system (boring bar), receive damped vibrations from the floating piece—a thin circular member designed to enable effective transfer of maximum vibrations between the curved surface of the boring bar and the flat end surface of the top spring. The absorber frame and floating piece, which are in direct contact with the boring bar, contribute to the absorber's damping performance.

The damping property of a TMD is primarily material-dependent, and optimal tuning is achievable by choosing the right material and 3D-printing properties such as infill density, pattern, and orientation. The flexibility to change the mass, stiffness, and damping properties of the TMD results in an optimal yet versatile passive vibration absorber unit. Figure 2 illustrates the boring bar–TMD system, along with the resultant forces and degrees of freedom, through a block diagram.

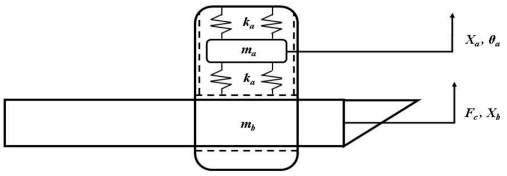


Figure 2. Schematic diagram of boring bar—TDOF TMD system.

2.3. Selection of Spring and Mass Parameters

A block mass weighing 30.8 g and a cylindrical mass weighing 6.6 g were fabricated using aluminium for the SDOF and TDOF TMD, as shown in Figure 3a. The springs for the SDOF and TDOF TMD were fabricated from stainless steel with dimensions and stiffnesses listed in Table 2, based on Equation (1).

$$K = \frac{G \cdot d^4}{8 \cdot D^3 \cdot n} \tag{1}$$

where, 'K' represents the spring stiffness, 'G' represents the shear modulus of spring material (Stainless Steel), 'd' indicates the spring wire diameter, 'D' signifies the mean coil diameter of the spring and 'n' implies the number of active coils. The fabricated springs for SDOF and TDOF TMDs are shown in Figures 3b and 3c respectively.

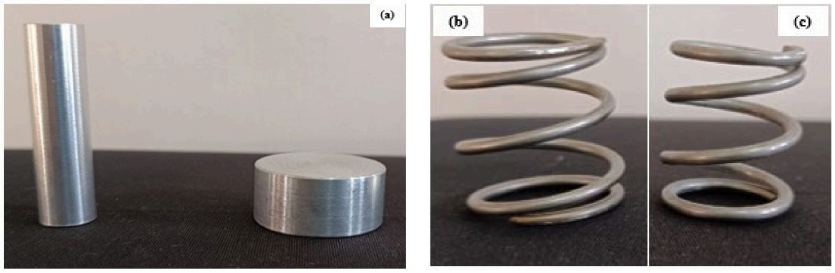


Figure 3. (**a**) Fabricated Aluminum masses; (**b**) springs for SDOF and (**c**) TDOF TMD.

Table 2. Table summarizing dimensions of fabricated springs for the TDOF TMD.

Spring	SDOF TMD	TDOF TMD
Material	Stainless steel (302)	Stainless steel (302)
Wire thickness (mm)	2.5	2.5
Effective number of coils	2	2
Length (mm)	30	30
Inner diameter (mm)	20	18
Mean coil diameter (mm)	22.5	20.5
Stiffness (N/m)	14,703	19,440
Effective absorber stiffness (N/m)	7351.68	19,440

The effective absorber stiffness values of the physical SDOF and TDOF TMDs as observed in Table 2 were determined based on their series and parallel combinations. The SDOF TMD consisted of two springs in series while the TDOF TMD consisted of two sets of parallel springs in series.

3. Theoretical Formulation

To achieve chatter control in the current boring problem, it is necessary to identify a set of independent variables that define the dynamic behaviour of the boring bar–TMD system. Identifying the optimum settings for these parameters is crucial in maximiszing the effectiveness of the proposed TMD model.

3.1. Finite Element Modelling of Boring Bar-Tuned Mass Damper System

The boring bar–TMD setup has been assembled as a continuous system in order to model the vibration behaviour as closely as possible. The boring bar has been modelled as a structural steel (density = 7850 kg/m^3, E = 1.8 × 1011 N/m^2, υ = 0.29 and structural damping ratio = 0.035) continuous Timoshenko beam with a diameter of 40 mm using 100 BEAM 188 elements corresponding to an element size of 1.5 mm with equally spaced nodes (101 nodes) and moderate mesh refinement with cubic interpolation throughout the entire length and constrained by a fixed support on the clamping end resulting in mesh convergence for 60, 80 and 100 elements at 1144.3 Hz. This higher order formulation allows to accurately model the bending and transverse effects while minimizing spatial discretization errors to generate a stable tool-tip FRF. The TMD is modelled using the mass element: MASS21 and spring-damper combination element: COMBIN14. At this juncture, it is worth highlighting that the PLA frame was not modelled as a part of the FE model of the boring bar–TMD system. Therefore, the specific material properties of PLA and the 3D printing parameters mentioned in Table 1 were not used as input parameters in the FE model. Therefore, the dynamic behaviour of the TMD system is governed by the lumped mass, equivalent stiffness, and damping coefficient values of the MASS21 and COMBIN14 elements. The properties and printing parameters listed in Table 1 are intended solely to reproduce the fabricated absorber components. Similarly, the numerical damping coefficient values used in the FE model are not to be associated with the material damping property of PLA.

The boring bar–TDOF TMD together consisted of 101 beam elements, two spring-damper elements and one rigid mass element distributed across 104 nodes. For the TDOF system, the absorber assembly consisted of an assembly of a rigid mass placed at the center of a 30 mm beam thus possessing translational and mass moment of inertia. Two spring-damper elements connected to the absorber at the ends of the distributed absorber mass (spatial separation) thereby facilitating restoring forces and moments. These constraints effectively restricted the motion of the absorber mass to the direction of dominant translational and rotational vibration modes. Hence the absorber was characterized by two coupled coordinates: transverse translation and small angular rotation about the out of plane z-axis. The rotational component of motion was a resultant of interaction between the distributed mass, separated spring-damper setup and rotational inertia rather than a simple eccentric mass. Similarly for the case of SDOF TMD system, all elements have been constrained to a 2-D inertial behavior along the transverse axis (y-axis) to ensure the system always vibrates along the dominant transverse axis. This assumption has been made as the transverse mode was observed to be the dominant mode during boring operation. The FE model of TDOF TMD systems has been shown in Figure 4.



Figure 4. Boring bar-TMD system modelled in ANSYS Mechanical APDL for TDOF TMD system.

3.2. Definition of Tuned Mass Damper Parameters

The parameters observed to influence the chatter behavior of boring bar-SDOF TMD system, and their range of values are shown in Table 3.

Table 3. Range of values for SDOF single TMD parameters.

Parameter	Description	Lower Value	Upper Value
Position (x)	Distance of TMD from tool tip	5 mm	75 mm
Mass ratio (mu)	Ratio of mass of TMD to the absolute mass of boring bar.	0.01	0.1
Frequency ratio (f)	Ratio of natural frequency of TMD to natural frequency of boring bar.	1.001	1.04
Damping ratio (zeta)	Damping ratio of TMD	0.001	0.2

The range of values for mass ratio, frequency ratio and damping coefficient of SDOF TMD were defined based on data obtained from the work of Sims [5]. The position of the TMD along the length of the boring bar was defined based on practical limitations in boring operation. The absorber parameters for TDOF TMD system and their range of values have been defined as shown in Table 4.

Table 4. Range of values for TDOF TMD parameters.

Parameter	Description	Lower Value	Upper Value
Position (x)	Position of spring-mass setup from tool tip	30 mm	75 mm
Stiffness (K)	Stiffness of spring away from tool tip.	2,900,000 N/m	3,300,000 N/m
Damping coefficient-1 (DC1)	Damping coefficient of spring-mass setup close to tool tip	300 N-s/m	700 N-s/m
Damping coefficient-2 (DC2)	Damping coefficient of spring-mass setup away from tool tip	50 N-s/m	350 N-s/m

In contrast to previously reviewed research work carried out on TDOF TMDs, some independent parameters of the absorber have been subject to constraints to maintain close resemblance to real-world absorber design limitations. The distance between the two springs (fixed inter-spring spacing) was assumed to be 30 mm which was also the length of the distributed mass. Hence the distributed mass was attached to the springs at its end. The stiffness of spring close to the tool tip was assumed to be 100,000 N/m lower than that of spring away from tool tip (stiffness coupling condition). This stiffness coupling condition was imposed as a design constraint rather than a tuning criterion with the main objective of simplifying the parametric design space by reducing the number of independent stiffness parameters while retaining two spring stiffnesses as in the original TMD while maintaining the practical simplification of two geometrically similar spring elements for the absorber. Spring with lower stiffness was placed closer to the tooltip to accommodate an increased relative motion at the location of higher modal displacement while the higher stiffness support away from the tooltip contributed as an additional restoring force. The 100,000 N/m offset was chosen as a sensible preliminary value considering the stiffness range and was not a product of any approach to determine an optimum value nor an experimental measurement.

The range of values for the two damping coefficients: DC1 and DC2 were chosen to consider absorber responses with various degrees of damping in the FE-model. A higher range of values for DC1 was assigned with an intention to attenuate the higher responses perceived closer to the tooltip while smaller values for DC2 were intended to avoid imposing excess restrictions on absorber motion. These coefficients were only intended as viscous damping elements in the FE-model and not to be considered towards the material damping property of the fabricated PLA-TMD frame.

Experiments within the design space were performed for a constant absolute mass ratio: absolute absorber mass to absolute boring bar mass (signifying fixed absorber mass and moment of inertia) of 0.09 (140 g) and corresponding moment of inertia of 1.13×10^{-5} kg-m^2 by framing a suitable range of values for each of the above-mentioned

parameters. Such constraints on absorber mass ratio, moment of inertia and inter-spring spacing were framed to consider practical engineering challenges in manufacturing an additively manufactured absorber. The dimensions of the cavity within the absorber frame were ascertained based on the available mounting space within the cavity. Moreover, the investigation of the influence of stiffness, damping distribution and absorber position could only be possible by maintaining a constant absorber mass and inter-spring distance. Introducing variability to such geometric and inertial parameters would enlarge and complicate the design space and diminish the individual effects of primary tuning parameters.

3.3. Construction of Stability Lobe Plots

Forced vibration analysis is performed for the boring bar-TMD system to study the response of system when subjected to external loading conditions within a specified frequency range. The response of system to harmonic loading is observed as a frequency response function (FRF), which is a plot of vibration amplitude to frequency of vibration. In this study, the amplitude of the negative real part of FRF is recorded and used as an input to optimize the limiting depth of cut in the stability lobe plot. The stability lobes were constructed using the FRF obtained from forced vibration analysis as an input to the expression of regenerative chatter stability in orthogonal cutting [38]. The Equations (2) and (3) are,

$$a_{lim} = \frac{-1}{2K_f G(\omega_c)} \tag{2}$$

$$N = \frac{60\omega_c}{2\psi + (2n+1)\pi} \tag{3}$$

where a_{lim} is used to denote limiting depth of cut, ψ signifies the phase angle connected to the regenerative delay effect between subsequent passes, n denotes the order of the stability lobe and K_f is the cutting force constant along the feed direction, considered as 2×10^9 N/m^2 based on the combination of structural steel boring bar and mild steel workpiece considered in the current work based on information presented in [38] and $G(\omega_c)$ represents the real part of the frequency response function. A stability lobe consists of the depth of cut (mm) plotted against the cutting speed (rpm). The depth of cut corresponding to the lowest point on the curve gives the limiting depth, which is the maximum safe depth of cut that can be employed during the cutting operation for all cutting speeds without being affected by chatter. The above explained methodology has been summarized in the form of a flow chart in Figure 5.

3.4. Optimization of Tuned Mass Damper Parameters Using Design of Experiments—Response Surface Methodology (RSM)

Response surface methodology is used to analyze the influence of each independent variable and the interaction between independent variables on the response variable (limiting depth of cut). RSM has been employed to achieve the primary objective of current work which is to develop a statistically valid surrogate model constrained by a well-defined physically bounded design space rather than to solve a highly multimodal global optimization problem. It is for this purpose that the independent parameter ranges were defined based on relevant engineering considerations and previous absorber tuning studies [5]. The RSM central composite design (CCD) with four distinct factors was defined to effectively explore the bounded design region. The model also proved effective in identifying statistically significant parameters and their interactions while also predicting an optimum parameter combination which returned the maximum limiting depth of cut. The analysis is performed based on a best fit cubic equation generated through a stepwise backward elimination procedure in Minitab Statistical Software 22. Beginning with all

model predictors, backward elimination gradually eliminates the least influential variable at each step. When all model variables have *p*-values that are less than or equal to the designated alpha-to-remove value, the process comes to an end. The alpha-to-remove value has been set as 0.05 in accordance with the 5% significance level criteria.

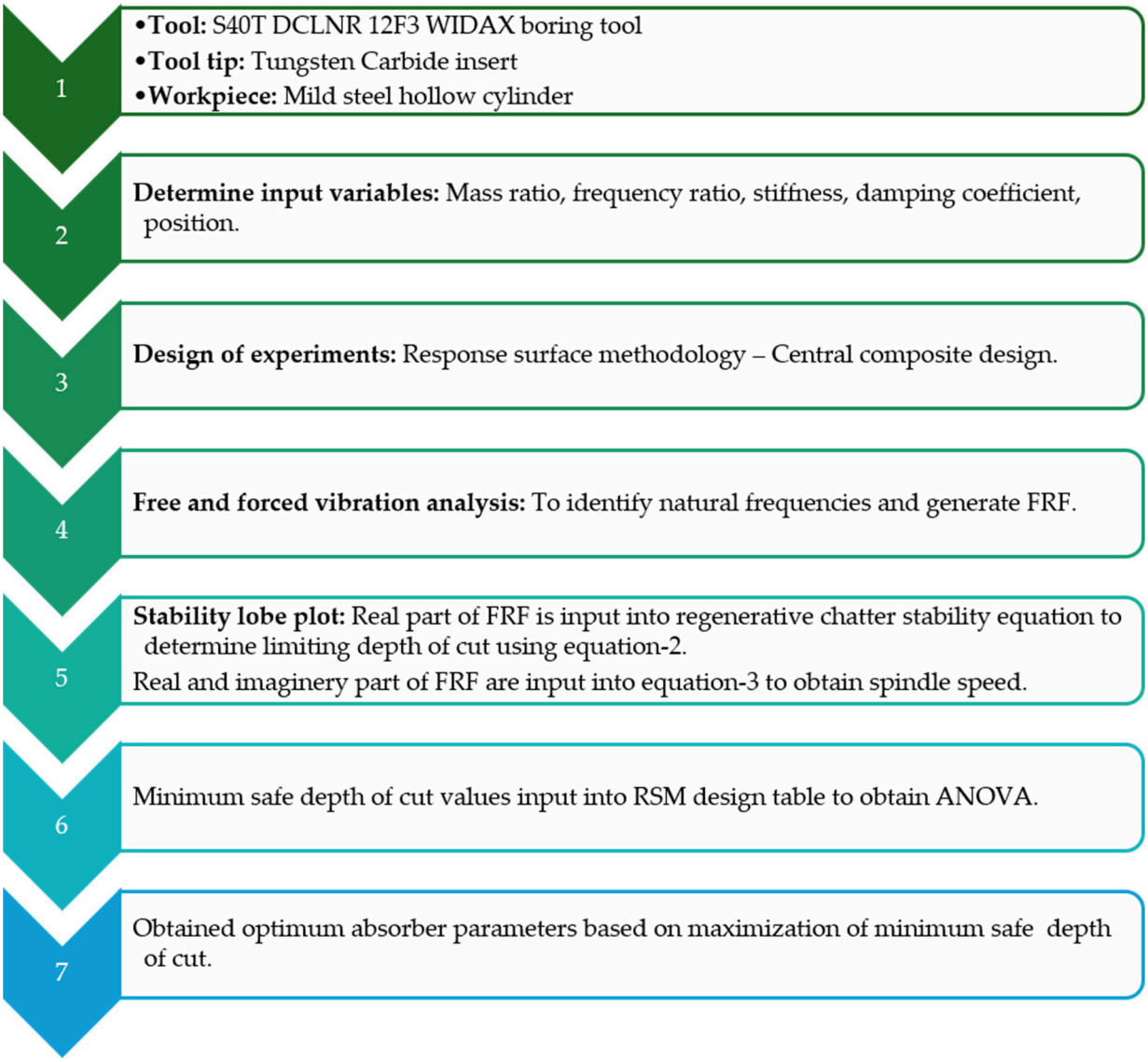


Figure 5. Flowchart summarizing the methodology.

4. Numerical Results

4.1. Free and Forced Vibration Analysis of Undamped and Damped Boring Bar System

The principal mode along the transverse *y*-axis was determined by performing free vibration analysis on the boring bar. The boring bar was observed to vibrate at a frequency of 1144.3 Hz. When performing free vibration analysis of the boring bar–SDOF TMD system, the principal mode of the undamped boring bar was observed to split into two bending modes: 1037.4 Hz and 1287.7 Hz, indicating the effectiveness of the SDOF TMD in controlling the principal mode of the boring bar along the transverse *y*-axis. Similarly, free vibration analysis of the boring bar–TDOF TMD system was performed to determine the bending and rotational modes of the system which together contribute towards effective suppression of the principal mode. The bending mode was found to be 917.8 Hz, and the rotational mode was found to be 1307.4 Hz. An analogous split in the original principal

mode of the boring bar, with the bending mode of the boring bar—TDOF TMD system falling just below the principal mode and the rotational mode slightly exceeding the same was observed as in the case of the SDOF TMD. This observation serves as a direct indication of effectiveness of the TDOF TMD in suppressing principal modes of boring bar. The various modes, their mode shapes and values have been listed in Table 5.

Table 5. Table to summarize the modes of the systems under study.

System	Mode	Natural Frequency (Hz)
Undamped boring bar system	Bending mode	1144.3
Boring bar-SDOF TMD system	Bending mode	1037.4
Boring bar-SDOF TMD system	Bending mode	1287.7
Boring bar-TDOF TMD system	Bending mode Rotational mode	917.8 1307.4

Figure 6 illustrates the bending and rotational modes of the boring bar-TDOF TMD system, observed through free vibration analysis.

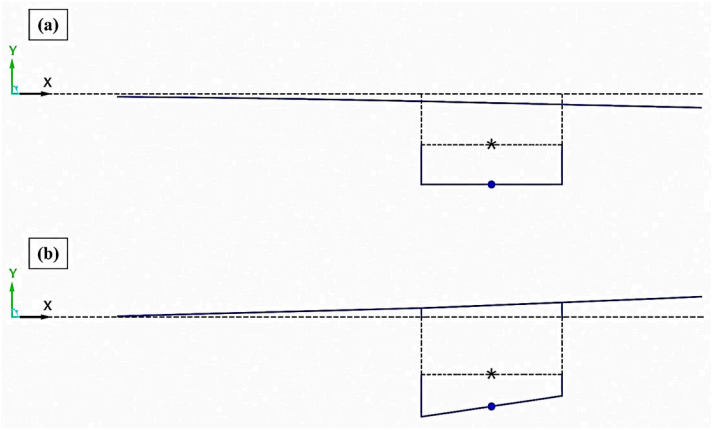


Figure 6. (**a**) Bending mode; (**b**) Rotational mode of boring bar-TDOF TMD system.

4.2. Optimization of Two-Degree of Freedom Tuned Mass Damper System

Analysis of variance was used to study how the input parameters and their higher-order interactions influenced the response variable (limiting depth of cut) based on the RSM model design of boring bar-TDOF TMD system. Based on the backward elimination procedure, the following terms could not be estimated and were removed from the analysis: x*x*K, x*x*DC1, x*x*DC2, x*K*K, x*DC1*DC1, x*DC2*DC2, K*K*DC1, K*K*DC2, K*DC1*DC1, K*DC2*DC2, DC1*DC1*DC2 and DC1*DC2*DC2. This resulted in a model with the final ANOVA containing only 10 model degrees of freedom. The response variable (DOC) values obtained for all generated design points in the RSM model of TDOF TMD are shown in Table 6 (For ease of understanding and homogeneity, the absorber position (x) has been listed out in cm).

The RSM design space consisted of 31 design points with seven center points at x = 5.25 cm, K = 3,100,000 N/m, DC1 = 500 N-s/m and DC2 = 200 N-s/m corresponding to the design point numbers: 2, 4, 6, 10, 18, 19 and 27 producing the same value of the FE-model-derived dependent variable DOC = 2.9781 mm. The exact repeatability in the response variables could be attributed to a deterministic FE-simulation model that governs the dynamic characteristics of the system that is replicated within a controlled environment with all variables under control. Within the RSM framework, the repetition of center points serves to fulfil the necessary central replication criteria and contributes towards estimation

of curvature within the RSM design space. It was observed that the average depth of cut obtained in the case of TDOF RSM model was higher than those obtained for a similar SDOF TMD RSM model, thus serving to verify the improved chatter stability provided by the TDOF TMD. The summary of ANOVA obtained for the TDOF TMD RSM model is shown in Table 7.

Table 6. RSM design table for TDOF TMD RSM model and their corresponding limiting depth of cut response.

x (cm)	K (N/m)	DC1 (N-s/m)	DC2 (N-s/m)	DOC (mm)
6.375	3,000,000	600	125	2.546
5.25	3,100,000	500	200	2.978
5.25	3,100,000	700	200	2.612
5.25	3,100,000	500	200	2.978
6.375	3,200,000	400	125	2.43
5.25	3,100,000	500	200	2.978
6.375	3,000,000	600	275	1.354
5.25	3,100,000	500	350	2.211
4.125	3,000,000	600	275	3.347
5.25	3,100,000	500	200	2.978
6.375	3,200,000	600	125	2.102
4.125	3,200,000	400	275	4.463
4.125	3,200,000	400	125	6.24
4.125	3,200,000	600	125	5.984
6.375	3,000,000	400	275	1.619
4.125	3,000,000	600	125	5.891
3.0	3,100,000	500	200	6.72
5.25	3,100,000	500	200	2.978
5.25	3,100,000	500	200	2.978
6.375	3,200,000	600	275	1.381
6.375	3,200,000	400	275	2.371
7.50	3,100,000	500	200	1.01
5.25	3,100,000	300	200	3.536
4.125	3,000,000	400	275	4.653
4.125	3,000,000	400	125	5.591
5.25	3,300,000	500	200	3.044
5.25	3,100,000	500	200	2.978
5.25	2,900,000	500	200	2.848
4.125	3,200,000	600	275	3.618
6.375	3,000,000	400	125	2.677
5.25	3,100,000	500	50	5.19

Table 7. ANOVA for TDOF TMD RSM model.

Source	DF	Adj SS	Adj MS	F-Value	*p*-Value
x	1	7.198	7.199	185.98	<0.001
K	1	0.225	0.225	5.80	0.026
DC1	1	0.063	0.063	1.62	0.218
DC2	1	5.17	5.17	133.56	<0.001
x*x	1	1.515	1.515	39.14	<0.001
DC2*DC2	1	1.018	1.018	26.29	<0.001
x*DC1	1	0.024	0.024	0.63	0.437
x*DC2	1	1.969	1.969	50.87	<0.001
DC1*DC2	1	0.545	0.545	14.09	0.001
x*DC1*DC2	1	0.365	0.365	9.42	0.006
Error	20	0.774	0.039		

Table 7. *Cont.*

Source	DF	Adj SS	Adj MS	F-Value	*p*-Value
Lack-of-Fit	14	0.774	0.055	*	*
Pure Error	6	0.000	0.00000		
Total	30	71.172			

It is generally observed that the ANOVA table displays information for only those variables which have a significant influence on the response variable. From the ANOVA, it is observed that the *p*-values of all independent factors are less than 0.05, which signifies that all individual parameters have a significant influence over the response variable. The model summary shown in Table 8 suggests that the obtained RSM model can adequately predict variations in the response variable (DOC).

Table 8. Model summary for TDOF TMD RSM model.

S	R-Sq	R-Sq (Adj)	R-Sq (Pred)
0.197	98.91%	98.37%	96.21%

An R-squared value of 98.91% indicates the capability of the model to account for any variability in DOC, thus inferring an adequate fit of the model with the data. The adjusted R squared value of 98.37% reaffirms the relevance of the parameters and their terms. The model also holds a very good capability to predict new data as reflected in the predicted R squared value of 96.21% being close to the R squared value. A standard error value (S = 0.197) signifies the deviation between predicated and actual values in the model. These metrics indicate that the obtained RSM model provides an accurate surrogate representation of FE-responses for a set of parametric combinations within the design space. It is worth highlighting that the conventional RSM model implemented in present study only serves as a local surrogate modelling technique and on its own, cannot determine every possible optimum solution within a nonlinear design space. The regression equation provides an expression by which the depth of cut can be predicted by considering the significant terms along with their regression coefficients representing the magnitude of influence. The regression equation in coded units used to predict variations in response variables is as shown below:

$$\begin{aligned}\text{DOC} = {} & 3.0102 - 2.9789\ x + 0.1934\ K - 0.5573\ DC1 - 1.2996\ DC2 + 0.911\ x{*}x + \\ & 0.747\ DC2{*}DC2 - 0.156\ x{*}DC1 + 1.403\ x{*}DC2 - 0.493\ DC1{*}DC2 + 1.208\ x{*}DC1{*}DC2\end{aligned}$$

The transformation criteria used to convert the uncoded variables to coded form are to subtract the midpoint of each parameter's range, then divide by half the range. The transformations are as follows:

$$x = (x - 5.25)/2.25 \quad (4)$$

$$K = (K - 3{,}100{,}000)/200{,}000 \quad (5)$$

$$DC_1 = (DC_1 - 500)/200 \quad (6)$$

$$DC_2 = (DC_2 - 200)/150 \quad (7)$$

Equations (4)–(7) were used to calculate the coded variable values corresponding to the physical center point: x = 5.25 cm, K = 3,100,000 N/m, DC_1 = 500 N-s/m and DC_2 = 200 N-s/m. The coded variables for the center point were obtained as x = K = DC_1 = DC_2 = 0. When these coded variables are substituted into the regression

equation in coded units, it returns a DOC = 3.0102 mm. This signifies the intercept of the coded coordinate system employed by the regression model. The actual FE-model generated response variable value at the physical center point is DOC = 2.9781 mm. This indicates a regression residue of approximately −0.0321 mm. This deviation of 0.0321 mm is small compared to the standard regression error of S = 0.197 and thus confirms that the fitted model predicts the center-point response adequately. Moreover, considering that the RSM model is fitted by a best-fit cubic equation, the generated regression function cannot be expected to pass through every design point on the design space under consideration. The consistency of the regression model's ability to predict responses for a combination of independent variables is demonstrated through the close agreement of the predicted response value of 3.0102 mm with the actual FE-model predicted response value of 2.9781 mm.

The influence of variation in each independent factor on the response variable (DOC) is studied using the main effects plot shown in Figure 7.

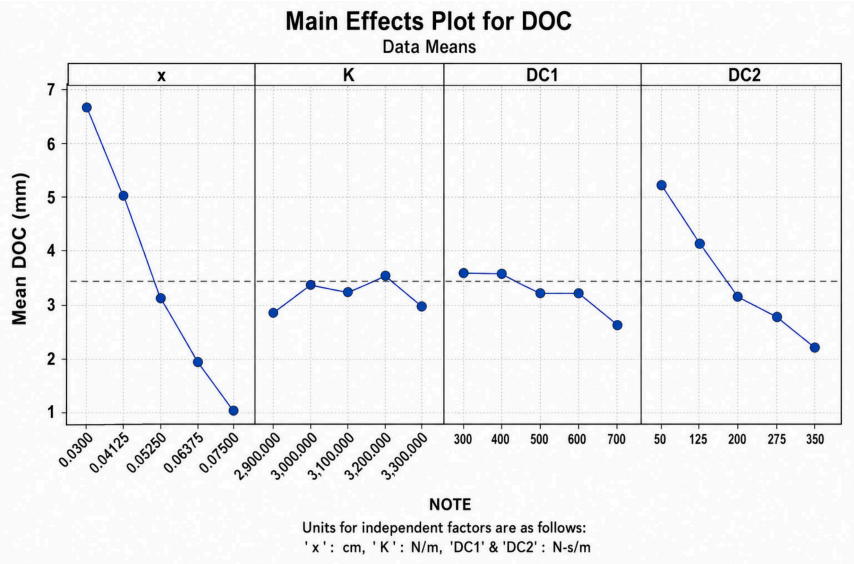


Figure 7. Main effects plot of TDOF TMD RSM model.

The low *p*-values (<0.001) and high F-values (185.98 and 133.56, respectively) for the parameters 'x'and 'DC2' highlight the higher individual influence of these independent parameters on the response variable and consequently on the chatter stability of the system. In contrast, 'K' and 'DC1', with a relatively higher *p*-value and lower F-value, indicate a weaker yet significant influence. Similarly, the quadratic terms of 'x' and 'DC2' are observed to exert a strong influence with significantly high F-values (39.14 and 26.29, respectively). High F-values for interactions between 'x', 'DC1' and 'DC2': 'x-DC2' (50.87), and 'DC1-DC2' (14.09) indicate a greater tendency for the absorber position and damping effects to exert influence through interactions. The interaction term 'x-DC1-DC2' with a smaller yet significant F-value of 9.42 further reinforces the observation that absorber position and damping coefficients are the most crucial parameters exerting a high strong influence both individually and through interactions. The main effects plot explains the independent influence of each parameter on the response variable. From the plot, it can be inferred that maximum depth of cut follows an inverse relation with the position (x) of the absorbers. It is observed that the limiting depth of cut decreases as the distance of the absorber from the tool tip increases. This directly indicates that better chatter stability is achieved by placing the absorber closer to the tool tip and the steep slope on the plot suggests that absorber position is the most influential parameter analogous to the insights from ANOVA. The effect of stiffness (K) is observed to be consistent across its range of variations with the depth of cut (DOC) encountering a mild peak at 3,200,000 N/m. This

makes stiffness (K) the least influential parameter. While damping coefficient near the tool tip (DC1) is observed to exert a moderate influence on the depth of cut with a slight increase (peak at 400 N-s/m) followed by a staggered decrease across its range of variation, the damping coefficient away from the tool tip indicates a negative slope. This indicates that an increase in DC2 inversely affects the depth of cut (DOC). This also suggests that applying excessive damping away from the tool tip impacts the chatter stability negatively. The cumulative effects of interaction between independent parameter pairs on the depth of cut are represented through a series of contour plots observed in Figure 8.

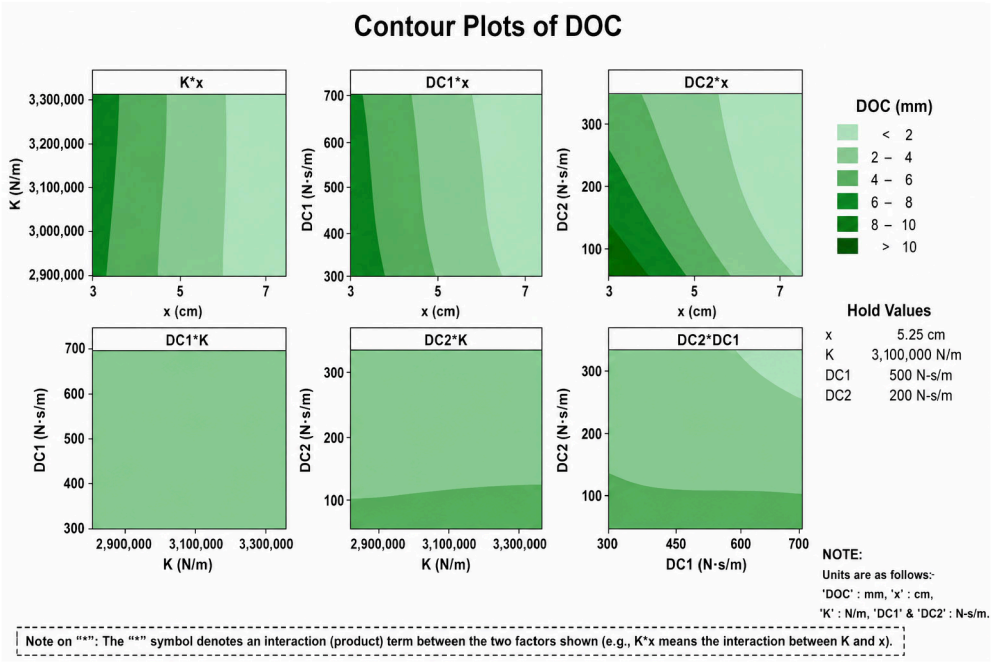


Figure 8. Contour plots of TDOF TMD RSM model.

From the K vs. x plot, it is observed that the DOC reaches its maximum value when the absorber is positioned close to the tool tip with stiffness having a minimal and homogeneous influence across its range of values, reinforcing the subsidiary influence of stiffness. Observing a strong gradient towards the lower values of absorber position with a moderately positive gradient towards the lower values of DC1 indicates that the DOC climbs towards lower values of x while maintaining an even gradient across the well-defined range of DC1. A very pronounced interaction is observed in the DC2 vs. x plot, with the DOC peaking at lower values of x and DC2 simultaneously. The DOC is also observed to be more sensitive towards variation in DC2 at higher values of x. A homogenous contour suggests a weak interaction effect between DC1 and K, suggesting a more pronounced influence of these parameters on the DOC rather separately. A minimal negative gradient exclusively along the DC2 axis suggests a moderate interaction effect between DC2 And K. It confirms the higher influence of DC2 as compared to K with the DOC observed to decrease with an increase in DC2 while simultaneously reaffirming the limited influence of K on DOC. The interaction between DC1 and DC2 is observed to follow a nonlinear gradient with DOC observed to peak almost uniformly across DC1 and at lower values of DC2. This further highlights the detrimental influence of excessive damping at DC2. The residual versus fitted values plot in Figure 9 conveys that the fitted values are scattered randomly about the reference line without any specific pattern, indicating that the residual variance is constant throughout the design space. This random distribution of variance across the design space satisfies the criterion for a constant variance across all values of independent variables.

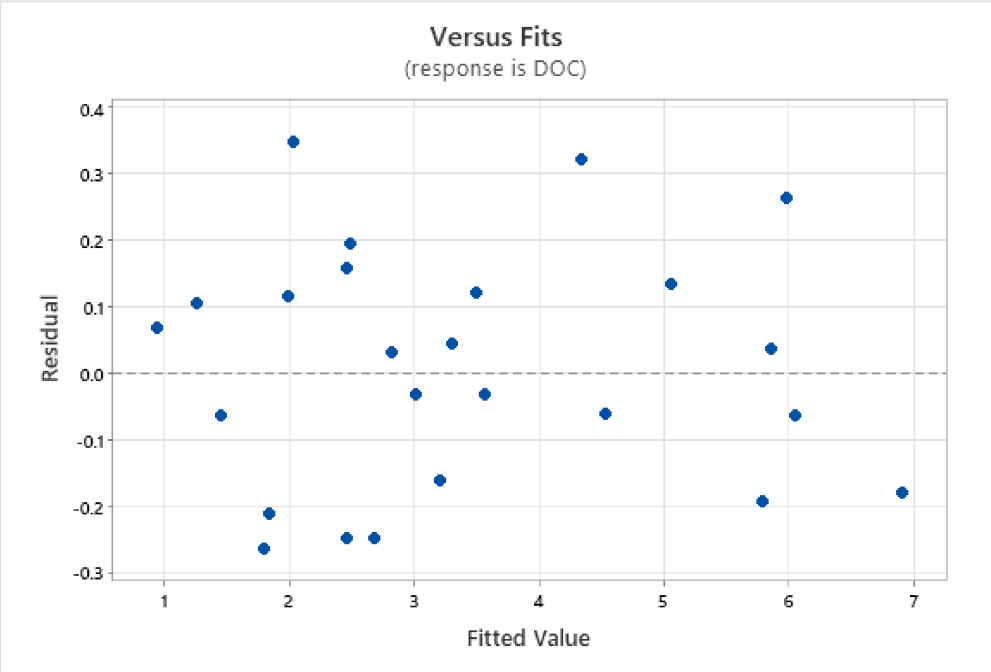


Figure 9. Residual plot of TDOF TMD RSM model.

Table 9 contains the optimized response variable value along with the corresponding combination of optimum independent parameters obtained based on the developed RSM model.

Table 9. Response optimization for TDOF TMD RSM model.

x	K	DC1	DC2	DOC Fit	Composite Desirability
4 cm	3,300,000 N/m	300 N-s/m	50 N-s/m	11.054 mm	1

From observing the response optimization for the TDOF TMD model in Table 9, it is worth noting that the RSM model converged on a constrained optimum at the boundary of the design space in the case of optimum values for K = 3,300,000 N/m and DC2 = 50 N-s/m. This predicted combination of optimum parameters is representative of the possible optimum solution considering the prescribed design space boundaries and does not represent a global optimum solution.

Based on the insights obtained from the main effects plot, contour plot and the response optimization, the range of optimum parameter values have been defined as follows:

- Position (x): 3–5 cm
- Stiffness (K): 3,200,000–3,300,000 N/m
- Damping coefficient-1 (DC1): 400–600 N-s/m
- Damping coefficient-2 (DC2): 50–150 N-s/m

A similar RSM model was used to optimize the SDOF TMD parameters by maximizing the limiting depth of cut. A comparison between the SDOF and TDOF TMD RSM models in Table 10 clearly suggests that the TDOF TMD RSM model can provide a more accurate prediction of the variations in limiting DOC as well as achieving a higher optimum depth of cut within the defined parameter range of values.

Table 10. Comparison of results obtained for SDOF and TDOF TMD RSM models.

Parameter	SDOF TMD	TDOF TMD	Percentage Increase
Average DOC	2.479 mm	3.364 mm	35.7%
Optimum DOC obtained using response optimization	4.335 mm	11.054 mm	155%
R-sq values in model summary	98.61%	98.91%	

Stability lobe diagrams for the design points generated by the RSM model and the optimum response were plotted using the real and imaginary part of the frequency response, obtained from free and forced vibration analyses performed in ANSYS Mechanical APDL 2026 R1. The tool-tip FRF was exported and used in a MATLAB R2026a code implementing the Altintas frequency-domain chatter stability equations to plot the resulting spindle speed—depth of cut pairs to obtain corresponding stability lobe diagrams. This is observed in Figure 10, which shows the limiting DOC achieved by the undamped SDOF and TDOF TMDs with optimum absorber parameters.

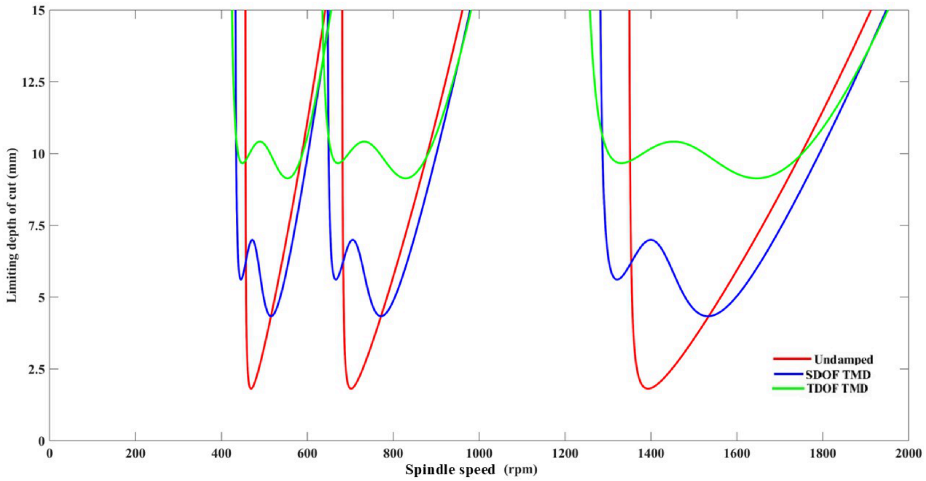


Figure 10. Stability lobe plots for systems with and without TMD.

The primary influence of SDOF and TDOF TMDs in the boring process could be verified by observing the significantly raised double-trough in the stability lobe plots of SDOF and TDOF TMDs in contrast to a single-trough in the case of an undamped boring bar system. This increase in the absolute stability limit is also inversely proportional to the most negative real part of the FRF, indicating the improved ability of the absorber to suppress vibrations of higher amplitudes. The single trough for the undamped boring bar system could be attributed to a single peak in the negative real part of the FRF. In contrast, a double trough signifies a split in the main system's natural-frequency mode into two smaller, separate modes, each corresponding to a new natural frequency. These double troughs in the TDOF TMD lobes are also observed to be higher and span a wider range of cutting speeds, allowing robust pockets of stability at higher spindle speeds than the undamped system. The average DOC for the SDOF and TDOF TMD RSM models is 2.479 mm and 3.364 mm, respectively. Because the two TMDs' design spaces were parameterised differently over dissimilar ranges, the average depth-of-cut values were mentioned solely to describe the distribution of the response variable within each design space. It was not meant to be interpreted as a performance metric to underline the superiority of the TDOF TMD over the SDOF TMD by virtue of its added degree of freedom. Rather, the associated stability lobes and FRF characteristics indicate how the respective TMD designs modify the system's dynamic behaviour. Consequently, the average DOC serves as a

descriptive indicator of the overall response surface of the design space. In contrast, the optimised response variable signifies the maximum response value achieved by the respective optimisation framework.

The improvement in broadband performance is attributed to the greater significance of absorber stiffness and the added contribution of the TMD's rotational mode, making the system less susceptible to detuning from random changes in machining parameters and conditions. Absorber stiffness is more significant in the TDOF TMD case. The TDOF TMD also shows shallower troughs, while the SDOF TMD shows deep, narrow lobes influenced by enhanced damping performance. The shallower set of lobes across a wider range of spindle speed speeds observed in the case of the TDOF TMD system also means an improved average limiting depth of cut value by virtue of the effect of the radius of gyration.

The troughs observed in the SDOF and TDOF TMD stability lobes are not merely a result of fitting an optimum response by applying an RSM optimiszation framework; rather, they have come to be as a result of the exploration of a design space of absorber parameters, which were selected and whose ranges were defined based on practical manufacturing constraints. This resulted in a surrogate model of the limiting depth of cut, physically bounded by the real part of the tooltip FRF based on Altintas's chatter stability equation [33]. Consequently, it can be accepted that maximiszing the DOC is analogous to minimising the most negative point on the real part of the FRF. In the case of the TDOF TMD, overall balancing of the FRF response improves dynamic compliance across the entire frequency domain, producing uniform (almost equal) troughs across all lobes. This inference is physically perceived as homogeneous energy transfer between the two ends of the absorber, better synchronisation between the stiffness and asymmetric damping elements, and robust chatter stability against unprecedented spindle speed variations.

These results also strongly agree with the ANOVA results and inferences. Through this interpretation of the current methodology, it is worth highlighting the point that the 'equal troughs' criterion, which has become the main cornerstone to qualify the optimisation of an absorber, is not explicitly instilled. That is, conventional absorber optimisation strategies like equal troughs, detuning, etc., employed in the work of Wang et al. [7] were not input as pre-constraints to the optimisation algorithm. Rather, it is the inherent objective of RSM model optimiszation. This highlights another perspective on the significance of the RSM model within the proposed absorber design optimisation methodology.

It is also worth stating that the 'equal trough' characteristic of the stability lobes of SDOF and TDOF TMD systems is dependent on determining the optimum combination of independent parameters, such as absorber position, stiffness and damping, and not an inherent property of a system damped using an absorber. Other common cases of suboptimal parametric combinations resulted in an unbalanced FRF, causing an unequal split in the fundamental undamped mode. This resulted in a stability lobe with pairs of deep and shallow troughs or, in worse cases, the loss of a trough. Poor damping distribution (high DC2 or small DC1) can result in an overdamped mode, significantly reducing the absorber's anti-resonance capability. This is perceived as a distorted trough shape. Suboptimal absorber positioning severely impacts modal participation. This compromises the absorber's ability to interact effectively with the tool's fundamental mode. This is reflected in asymmetric trough depths. Hence, it could be inferred that optimal damping (resulting in equal troughs) requires the following prerequisites:

- Optimal positioning of the absorber
- Appropriate stiffness tuning within the range of the fundamental mode of the tool-workpiece system.
- Asymmetric and optimally distributed damping.

4.3. Observations and Inferences from RSM Model Design Space

The stability lobes obtained for design points generated by the RSM model revealed that the 'nearly equal double trough' is not obtained for most design points. Among the 31 design points, it is observed that almost all combinations of independent parameters returned a clear single-trough shape on the stability lobe curve. This serves to infer that a random combination of independent parameters does not ensure effective dynamic stability, observed as a dual mode interaction in the case of a two-degree of freedom absorber. This observation is justified by the fact that these design points are generated by the RSM model with the primary goal of exploring the entirety of the design space statistically and not with the intention to ensure optimum dynamic stability.

On the other hand, the optimized response predicted by the RSM model after model-fitting and ANOVA is a result of the model's ability to determine statistically significant influences from the independent parameters, thus returning an optimum combination that does not correspond with any of the generated design points. It represents an interpolated set of parameters within the defined limits of the design space that assert an optimally balanced contribution from all parameters cumulatively. Dynamically this is reflected as the real part of FRF reorganized effectively within the vicinity of the intended bending mode frequency, consequently resulting in a nearly equal double-trough.

Focusing beyond the primary purpose of design points generated by the RSM model to determine the optimal set of parameters, the design points further serve to realize the influence of each parameter on the system's dynamic stability, determined by the negative real part of the FRF, the limiting depth of cut obtained from the stability lobe diagram and the topology of the stability lobe. The 31 parameter combinations generated by the RSM model produced significant heterogeneity in depth of cut and stability lobe shapes. Furthermore, the lobe topology transforms as the limiting depth of cut increases. Figure 11 shows the variations in lobe topology for six design points, with returned depths of cut from 1 mm to more than 6 mm.

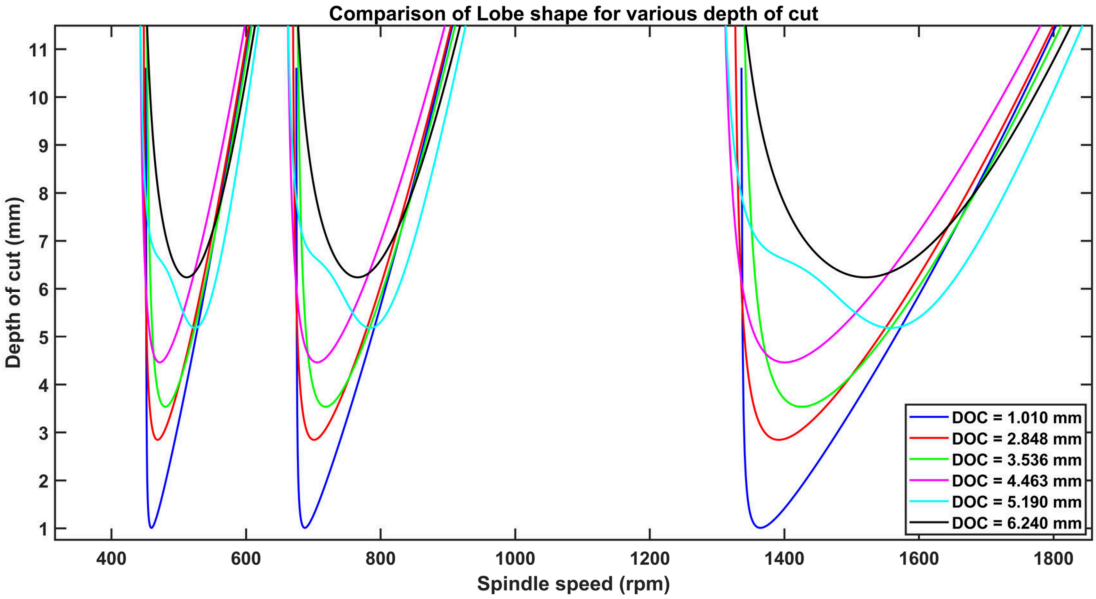


Figure 11. Transformation in lobe topology with an increase in limiting depth of cut.

An increase in depth of cut analogous to a reduction in the negative peak of the real part of the FRF clearly translates into a lobe that rests at a higher minimum depth of cut, along with a gradual increase in the range of permissible cutting speed. It is also worth noting that the bottom of the trough progressively widens. This observation also

agrees with the tendency of lobes to span a wider range of stable cutting speed speeds with improved chatter stability. Similarly, the reduction in the negative real part of FRF from nearly -0.7×10^{-6} m for a design point with DOC of 1.01 mm to approximately -1.2×10^{-7} m for a design point with DOC of 6.240 mm as seen in Figure 12 indicates the progressive improvement in coupling of the absorber with the fundamental bending mode of the tool, which consequently results in the upward shift in the stability lobe.

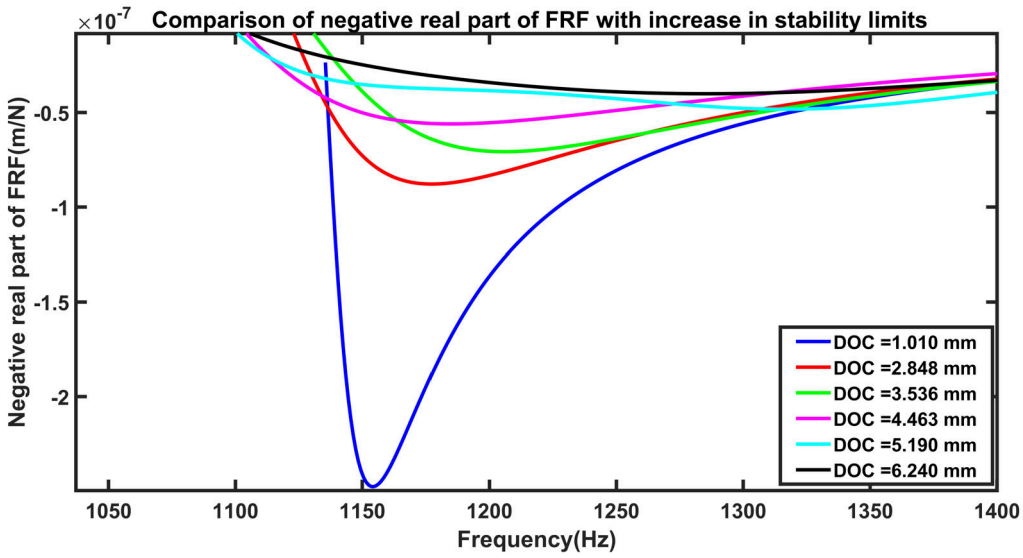


Figure 12. Reduction in negative real part of FRF with an increase in stability limit.

From the RSM design points, examining points 17, 2, and 22 provides insights into how variation in absorber position 'x' influences the limiting depth of cut and lobe shape. Modal participation of the absorber improves significantly as the absorber moves closer to the tool tip, influencing the tool-tip FRF more prominently and reducing its negative real part. From Figure 13, it can be noted that the position of the stability lobes tends to shift upwards and occupy a wider stable region as the position of the absorber is moved through x = 0.075 m, 0.0525 m and 0.03 m (maintaining other parameters as: K = 3,100,000 N/m, DC1 = 500 N-s/m and DC2 = 200 N-s/m) thus exhibiting a progressive improvement in the stability boundary.

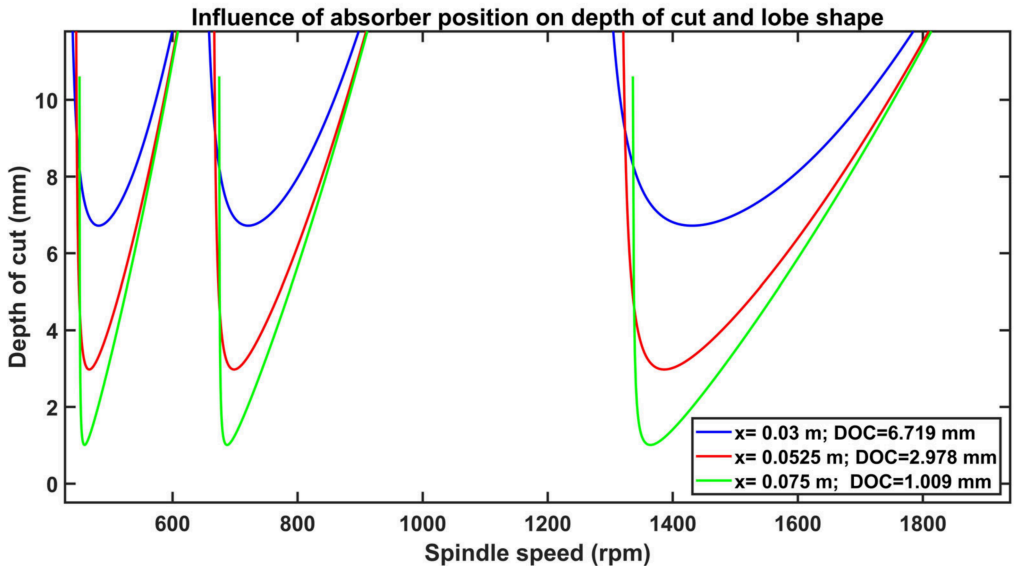


Figure 13. Influence of absorber position on depth of cut and lobe shape.

Generally, stiffness contributes towards dynamic stability by influencing the absorber tuning relative to the resonant bending frequency of the tool because the natural frequency of the absorber is directly attributed to its stiffness. The effect of stiffness 'K' on the depth of cut and lobe shape can be interpreted by examining the design points: 25 and 13 with stiffnesses K = 3,000,000 N/m and 3,200,000 N/m, respectively, while other parameters were maintained constant at x = 0.04125 m, DC1 = 400 N-s/m and DC2 = 125 N-s/m. The increase in limiting depth of cut from 5.591 mm to 6.240 mm (11.6% improvement) could be attributed to its improved contribution towards coupled system dynamics. From Figure 14, the stability lobes are clearly distinguishable by an upward shift in trough depth (improved depth of cut) and widening of the range of stable cutting speeds.

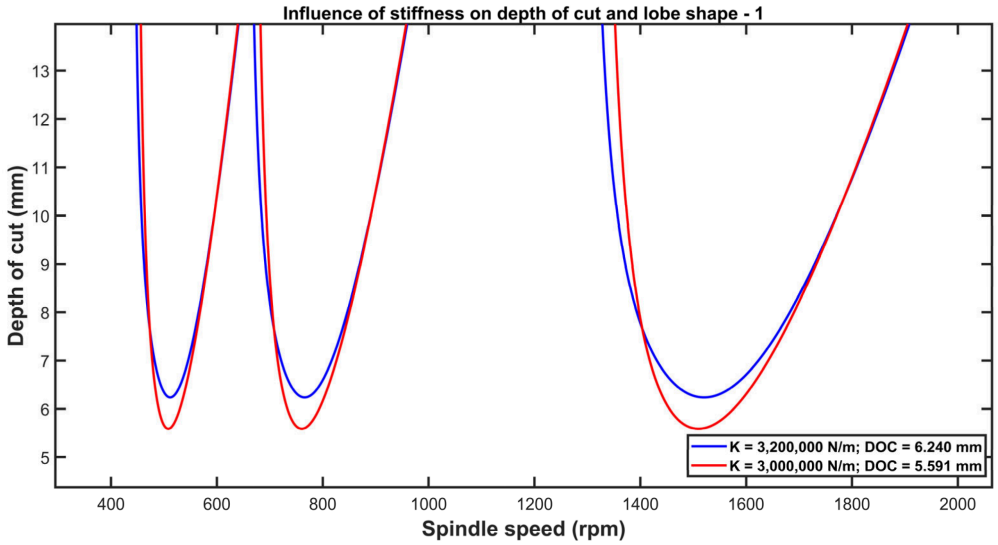


Figure 14. Influence of stiffness on depth of cut and lobe shape-1.

This observation indirectly indicates that the relative tuning of the absorber improves with an increase in absorber stiffness. However, the extent of the influence of absorber stiffness is highly dependent on optimal absorber placement and damping distribution. This contrasting nature of the influence of 'K' is better understood by examining another set of design points with suboptimal absorber placement and damping distribution resulting in a weaker influence of absorber stiffness 'K'. The design points: 28, 2 and 26 are considered where constant parameters are maintained at x = 0.0525 m, DC1 = 500 N-s/m and DC2 = 200 N-s/m with stiffness varying as K = 2,900,000 N/m, 3,100,000 N/m and 3,300,000 N/m respectively. In this case, a significant increase in stiffness only results in a nominal increase in depth of cut from 2.848 mm to 3.044 mm (an improvement of 6.9%). Looking at Figure 15, the lobe shapes remain almost identical with a minimal upward displacement of the troughs.

This points towards inadequate modal coupling and decreased modal participation because of suboptimal absorber placement. These insights serve to reiterate the previous inference that absorber stiffness 'K' cannot be considered as an independently dominant parameter; rather, it can be considered as an essential component towards tuning an absorber whose effectiveness depends on optimal absorber position and damping distribution.

We study the influence of 'DC1' by examining the depth of cut and lobe shapes of design points: 13 and 14 with constant parameters defined as x = 0.04125 m, K = 3,200,000 N/m, DC2 = 125 N-s/m and DC1 = 400 N-s/m and 600 N-s/m respectively. In this case, the limiting depth of cut is observed to diminish from 6.240 mm to 5.984 mm (4.11% reduction). This observation agrees with the earlier inference on the detrimental effect of increasing DC1 excessively beyond an optimal range, as it could restrict the relative motion between the TMD

and the boring bar at the surface of contact. This inhibits efficient vibrational energy transfer between the source structure and the absorber, hence impeding effective energy dissipation. On observing Figure 16, it is clear that the lobes of design point 13 occupy slightly higher troughs and wider stable cutting zones with similar lobe shapes as compared to those of design point 14, implying that DC1 only exerts a moderate influence for the parameter set.

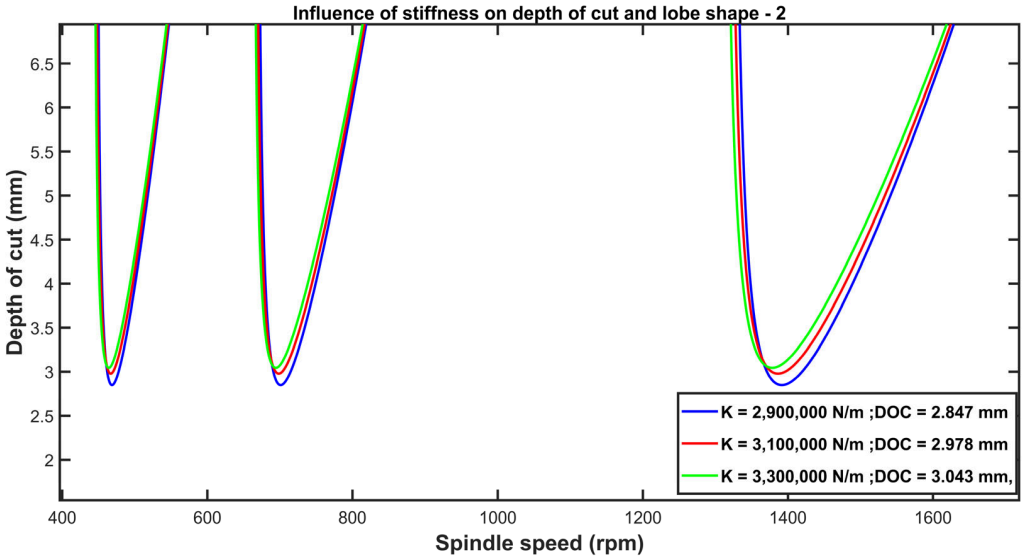


Figure 15. Influence of stiffness on depth of cut and lobe shape-2.

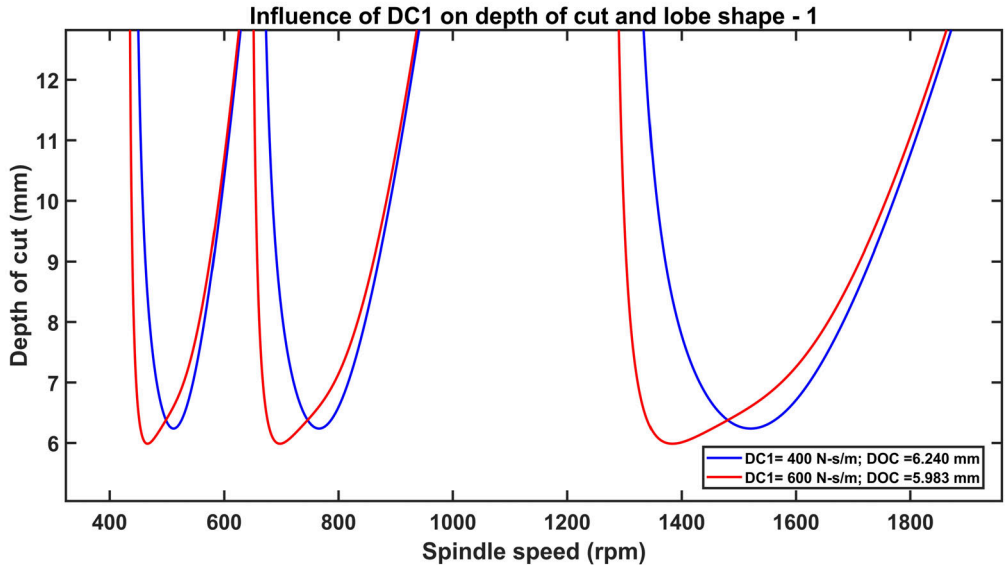


Figure 16. Influence of DC1 on depth of cut and lobe shape-1.

Hence, it is safe to label DC1 as an optimization-dependent parameter that further enhances stability at a particular range rather than being capable of independently enforcing significant influence like absorber position 'x'. This inference makes more sense when considering the role of DC1 in another set of design points: 23, 2 and 3, whose constant parameters are held at x = 0.0525 m, K = 3,100,000 N/m and DC2 = 200 N-s/m with DC1 values set at 300, 500 and 700 N-s/m. As noted in Figure 17, the limiting depth of cut is observed to decrease from 3.536 mm to 2.612 mm with minimal changes in lobe structure.

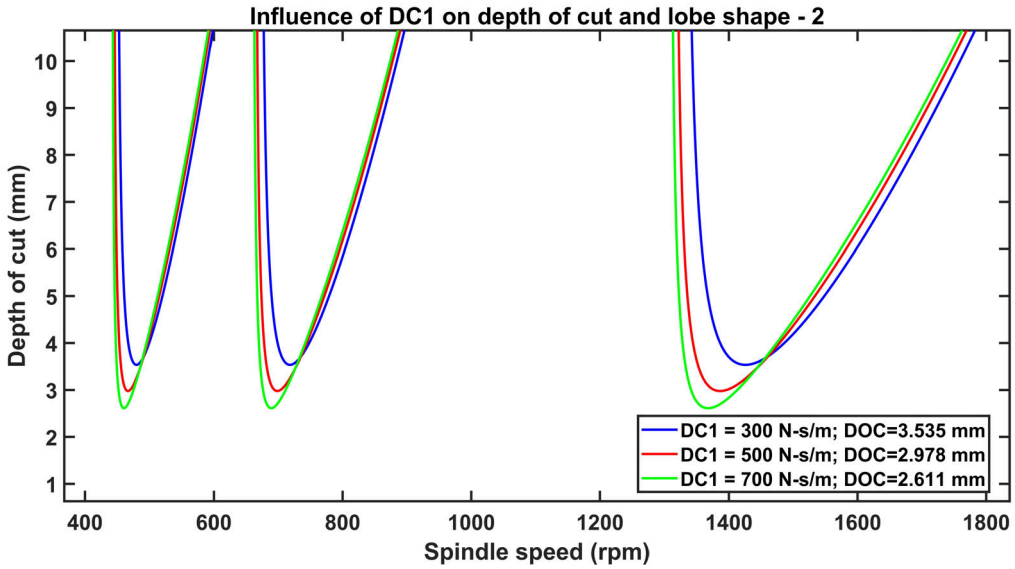


Figure 17. Influence of DC1 on depth of cut and lobe shape-2.

This example further reinforces the limited capability of DC1 to influence the modal coupling between the absorber and tool. In such cases of moderate modal participation, DC1 primarily tends to affect the damping magnitude of the existing coupled modes rather than bringing about a significant shift in FRF or changes in lobe shape. Hence, it produces minimal vertical shift in the stability boundary.

The stronger influence of DC2 on depth of cut and lobe topology is clearly observed by studying the following set of design points: 31, 2 and 8 with parameters held constant at x = 0.0525 m, K = 3,100,000 N/m, DC1 = 500 N-s/m with DC2 varied as 50, 200 and 350 N-s/m respectively. Figure 18 shows a very clear drop in depth of cut values from 5.19 mm to 2.978 mm and 2.21 mm, underlining the substantial dependence of the absorber's chatter stability on DC2.

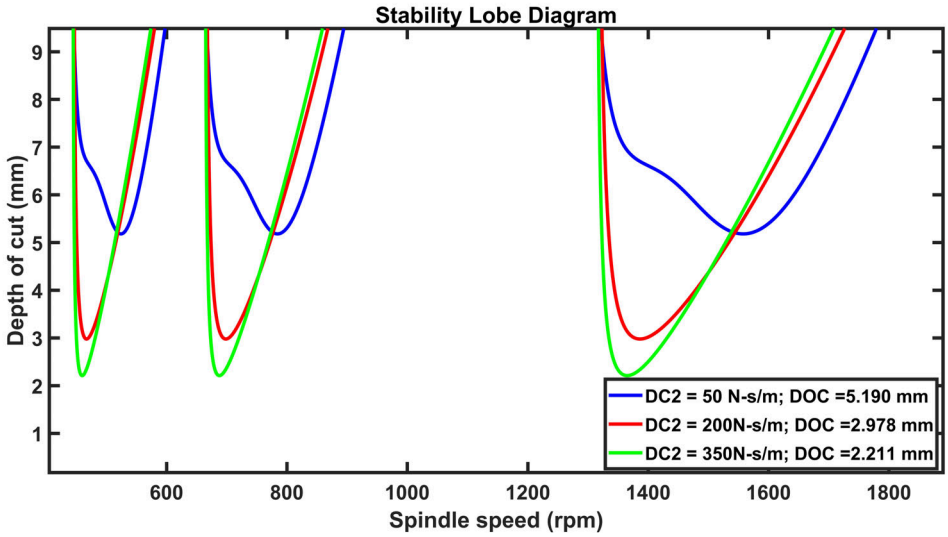


Figure 18. Influence of DC2 on depth of cut and lobe shape.

The design point: 31 with DC2 = 50 N-s/m results in a lobe placed higher than the other two lobes with deeper troughs, indicating effective relative motion at the TMD-boring tool interface. Having a lower damping setting allows the absorber to be more responsive to minor variations in chatter amplitude and thus provides effective attenuation of the primary resonant mode. The excessive damping of DC2 = 200 and 350 N-s/m moves the

lobes further downwards, making the lobes narrower, negatively affecting the stability limit due to a weak dynamic tuning effect, consequently making the absorber over-damped. This makes DC2 a very sensitive parameter.

5. Experimental Setup

Experiments to study the cutting stability of boring operations were performed using an S40T DCLNR 12F3 WIDAX boring tool with a 150 mm overhang under undamped and damped conditions. Mild steel hollow cylinders with inner and outer diameters of 95 mm and 110 mm, respectively, and a length of 70 mm were used as the workpiece. A lathe machine was used for boring operations. The workpiece was mounted onto a four-jaw chuck. The machining parameters were kept constant at a speed of 400 rpm, a feed of 0.2 mm/rev, and a depth of cut of 0.5 mm. While an aluminum mass block with a mass ratio of 0.02 (mass = 30.8 g) and stainless-steel springs with an inner diameter of 20 mm were used for the SDOF TMD, a cylindrical aluminum mass of 6.6 g (mass ratio = 0.004) and stainless-steel springs of 17 mm inner diameter were used for the TDOF TMD. The difference in absorber mass configuration used in the fabricated SDOF and TDOF TMDs is justified by the distinction between their corresponding TMD structures and associated practical design constraints. The TDOF absorber and geometry were designed to include translational and rotational inertia while remaining within the available cavity space, fixed inter-spring distance, and fabrication constraints of the additively manufactured TMD frame. Therefore, the purpose of experimental validation was to evaluate the chatter stability performance of two independently designed TMDs, rather than to verify the effect of added degrees of freedom by maintaining a similar mass value. Hence, an improved response was attributed to the combined effects of absorber mass, rotational inertia, coupled dual springs, and parametric tuning.

Varying absorber parameters tuned the TMDs, and their corresponding cutting stability was analyzed based on time-domain acceleration responses, power spectrum and spectrogram, with the main objective of validating the dynamic behavior predicted by the model through characteristic observations like mode splitting, frequency redistribution and vibration attenuation, rather than to validate optimum machining parameters obtained through the proposed optimiszation framework and numerically predicted stability lobe diagram. The experimental validation in this work aimed to validate the physical influences behind the observed stability improvement rather than replicate the machining process at the obtained optimal depth of cut. This is because the determined optimal limiting depth of cut represents the onset of chatter rather than a specific machining scenario.

The acceleration signals, spectrograms, and power spectra are used to evaluate vibration attenuation and the redistribution of dominant chatter frequencies, showing a shift in dominant spectral peaks that indicates modified dynamic behaviour due to tool-absorber coupling. These observations provide evidence of frequency redistribution under the influence of the TMDs. However, they are not to be interpreted as a substitute for EMA and direct FRF response validation. The experimental validation in the present work was intended only to examine how the respective physical TMDs modified the system's dynamic behaviour and, alternatively, does not validate the predicted enhancement in the chatter stability limit of the numerically optimised TMD. The experimental investigation in the present work is also not to be interpreted as validation of the numerical model's free and forced vibration response predictions. Moreover, experimentally validating a limiting depth of cut of 11 mm for a TDOF TMD system is practically infeasible for the boring setup used in the present work due to limitations in machine-tool power, tooling, and the workpiece.

The dynamic response of the system was acquired by mounting a Kistler Type 2825A-03 accelerometer (Kistler Instrumente AG, Winterthur, Switzerland) on to the boring bar directed

along the direction of feed with a range: ±2000 g, sensitivity of 2.5 mV/g, Sampling Frequency of 0.7 to 15,000 Hz and the vibration signals were captured through a KiNOVA Lite Type 5809A10 DAQ system with a maximum sampling rate of 144 kSps, 24-bit resolution, voltage range of ±95 mV to ±25 V and noise floor of −130 dB and requires the KiNOVA Capture/Basic Acquisition Software Acquisition software (Kistler Instrumente AG, Winterthur, Switzerland) to capture real-time frequency and time-domain signals. The proposed TDOF TMD model and a conventional SDOF TMD, modelled based on the TDOF TMD design configuration, both fabricated under similar printing parameters were experimentally investigated to perform a comparative analysis of their chatter stability performance under similar machining conditions. The experimental setup is as shown in Figure 19.

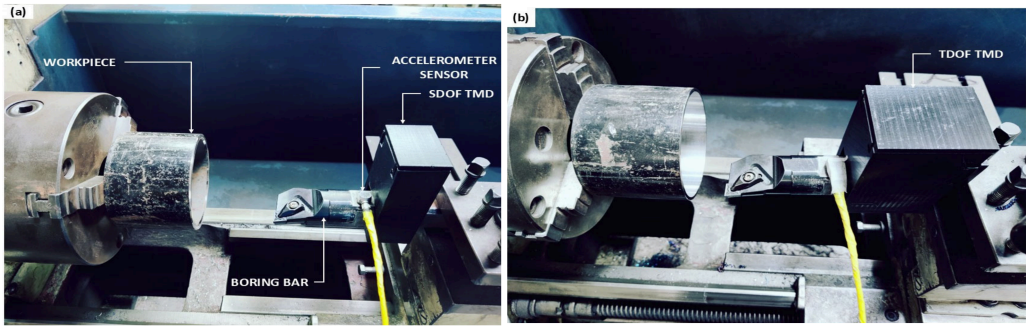


Figure 19. (**a**) Experimental setup of boring bar-SDOF TMD system; (**b**) Experimental setup of boring bar-TDOF TMD system.

The various parameters involved in the present study have been distinguished based on their purpose in the study in Table 11.

Table 11. Summary table for parameters.

Category	Parameters	Purpose
Measured/experimental parameters	Physical spring stiffness, absorber masses, TMD dimensions, Printing parameters (Elastic modulus, Structural damping coefficient)	Fabrication and characterization of prototype
Equivalent FE-model parameters	SDOF TMD: absorber position, mass ratio, frequency ratio, damping ratio. TDOF TMD: absorber position, stiffness, damping coefficients (DC1 & DC2). TDOF TMD boundary conditions: fixed inter-spring spacing, stiffness coupling, fixed mass ratio	Employed in ANSYS APDL FE-model as independent absorber parameters
Optimization parameters	Independent variables (TDOF TMD FE-model parameters): x, K, DC1, DC2. Response variable: depth of cut (DOC)	Parameters used in DOE (RSM-CCD) optimization
Calculated parameters	Natural frequencies, FRF, limiting DOC, stability lobes	Determined through FE analysis and Altintas stability model
Experimental parameters	Time-domain acceleration signals, power spectra, spectrograms	Experimental validation of dynamic behaviour of TMDs

6. Experimental Results

The dynamic performance of the SDOF and TDOF TMDs was analyzed and compared by plotting time-domain acceleration response curves, power spectrum and spectrograms. Time-domain acceleration curves were used to observe the state of vibrational amplitude of the system with SDOF and TDOF TMDs. From Figures 20 and 21, it can be observed that

the acceleration amplitudes of both SDOF and TDOF TMD configurations remain constant and bounded, signifying stable cutting conditions.

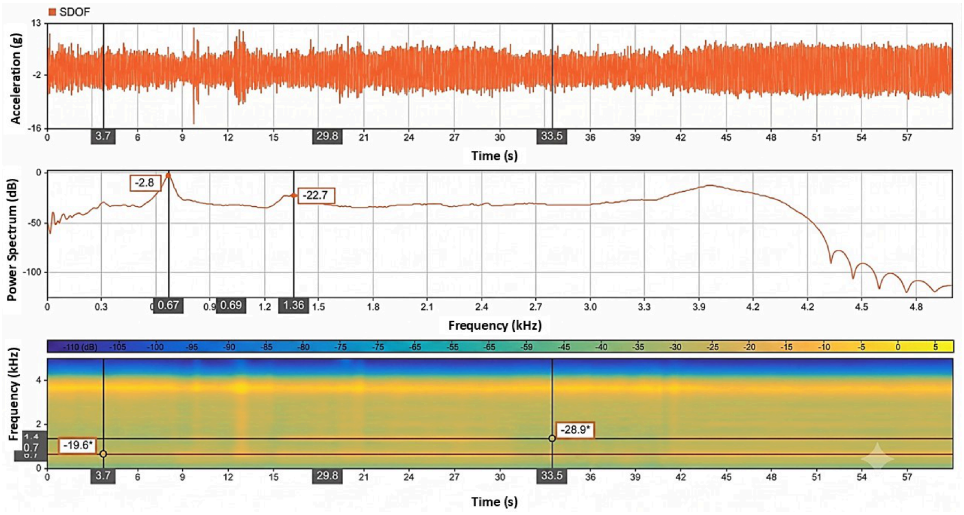


Figure 20. Time-domain acceleration response, power spectrum and spectrogram plots of SDOF TMD.

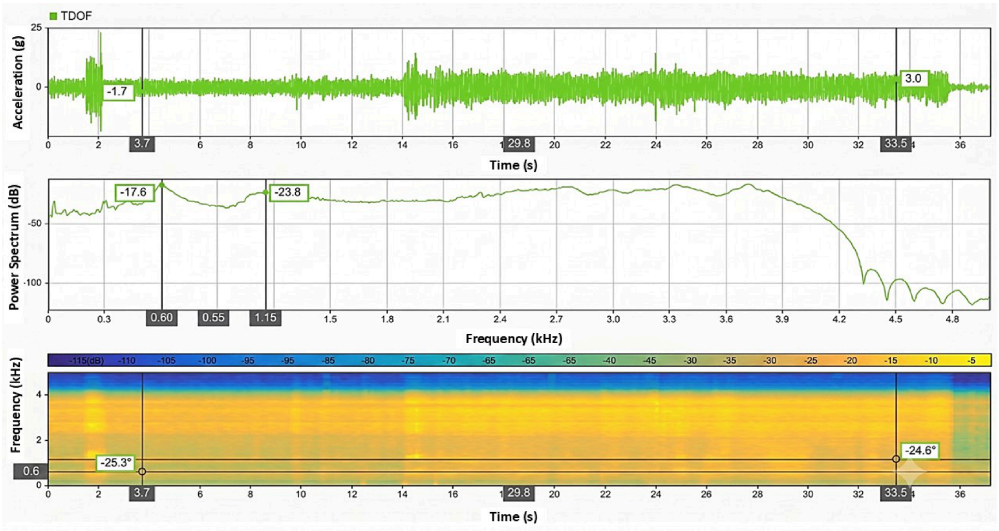


Figure 21. Time-domain acceleration response, power spectrum and spectrogram plots of TDOF TMD.

The time-domain acceleration signals of both TMDs were superimposed to compare their corresponding damping performances. The average time-domain acceleration amplitude of the TDOF TMD system was observed to be lower than that of the SDOF TMD system, as seen in Figure 22, confirming the superior chatter resistance capability of the TDOF TMD over the SDOF TMD.

Insights into the effectiveness of SDOF and TDOF TMDs are revealed through a power spectrum analysis with a unit reference level. When an absorber is integrated into a machining tool system, the power spectrum maps out continuous stable cutting oscillations along with its characteristic energy spikes analogous to chatter resonant oscillations, indicated by two smaller damped peaks at specific spindle speeds, directly associated with a double-trough response on the system's FRF at new absorber-coupled frequencies. On examining the power spectrum corresponding to the SDOF TMD system as seen in Figure 20, the first dominant peak is encountered around the value of 0.67 kHz, analogous to an amplitude of −2.8 dB. This excitation peak is further attenuated in the case of the TDOF TMD system as observed through the power spectrum in Figure 21, where the amplitude of

the first coupled frequency peak encountered around a similar frequency value (0.6 kHz) is −17.6 dB. This reaffirms the significant improvement in the system's chatter stability through the implementation of a TDOF TMD. Furthermore, the secondary peak of −22.7 dB observed at 1.36 kHz for the SDOF system also shifted to −23.8 dB at 1.15 kHz in the case of the TDOF system, demonstrating a superior efficiency of the TDOF TMD in redistributing coupled modes over that of the SDOF TMD.

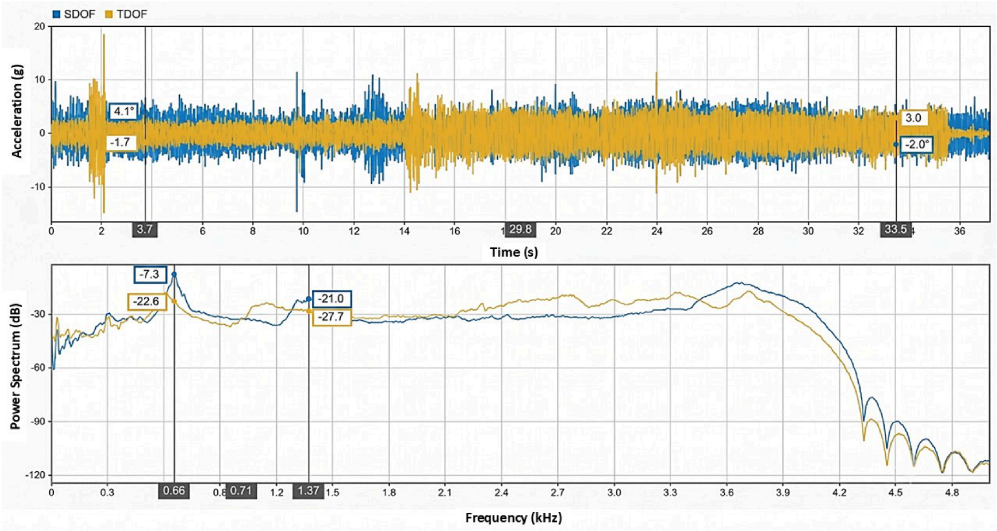


Figure 22. Comparison of time-domain acceleration responses and power spectra of SDOF and TDOF TMDs.

A spectrogram analysis combines information from the time-domain curve and the power spectrum to depict how the frequency of the vibrating boring tool evolves with time. In the case of SDOF TMD system, continuous high-energy regions are observed in the vicinity of resonant frequencies throughout the duration of cutting. This points towards a greater tendency of the SDOF TMD system to experience prolonged periods of exposure to unstable resonant modes. This contrasts with a lower spectral intensity for the same frequency range in the case of the TDOF TMD system, once again pointing towards effective modal redistribution and damping of resonant modes. The spectrogram of the TDOF system also represents a shorter duration of exposure towards higher energy frequencies highlighting the improvement in dynamic stability. The time domain acceleration responses, power spectrum and spectrogram manage to highlight the qualitative redistribution of structural dynamics by exhibiting new coupled resonance peaks rather than a comparable numerical redistribution as observed in Table 12 and a significant reduction in vibrational energy at dominant chatter frequency. These observations are analogous with the model's prediction of splitting the fundamental bending mode, directly reflected in the tool-tip FRF and a reduction in negative real part of the FRF indicating an improved chatter stability limit.

Table 12. Comparison of FE-model predicted and experimentally measured spectral peaks.

System	FE-Model Predicted Natural Frequencies (Hz)	Experimentally Measured Spectral Peaks (Hz)
SDOF TMD system	1037.4, 1287.7	670, 1360
TDOF TMD system	917.8, 1307.4	600, 1150

At this stage, it is worth noting that the optimized FE model of TMDs and the additively manufactured TMDs cannot be interpreted as dynamically identical. The purpose of

the experimental validation carried out in the present work was to examine the qualitative dynamic behavior demonstrated by the TMDs—the phenomenon of vibration attenuation and redistribution of natural frequencies. The additively manufactured physical TMDs were not meant to be an exact physical realization of the TMD designs obtained through the hybrid FE-RSM optimization approach due to constraints in physical spring stiffness, absorber masses, dimensional constraints, and manufacturing considerations, and as a result do not represent an exact physical manifestation of the absorber representing the optimum configuration. Consequently, experimentally measured frequency splits of the physical TMD systems cannot be expected to match those of the numerically optimized TMD system quantitatively. The natural frequency split observed for the numerically optimized TMD system was 932.3 Hz and 1329.9 Hz, with corresponding frequency ratios of 0.815 and 1.162 relative to the fundamental mode of the boring bar (1144.3 Hz). The corresponding frequency split for the physical TMD system was 600 Hz and 1150 Hz, resulting in frequency ratios of 0.524 and 1.005, respectively. When a similar boring bar–TMD system, modelled to represent the physical TMD system, was analyzed using a corresponding FE model, the resulting frequency ratios were 0.572 and 1.04. Table 13 summarizes the natural frequency splits and corresponding frequency ratios for each of the above-mentioned systems.

Table 13. Comparison of frequency splits and ratios for numerically optimized and physically fabricated TMDs.

	Frequency (Hz)	**Frequency Ratio w.r.t Natural Frequency of Boring Bar (1144.3 Hz)**
Frequency peaks after attachment of numerically optimized TMD—optimum FE-model	932.3 1329.9	0.815 1.162
New frequency peaks after attachment of physical TMD—FE results	654.72 1190	0.57 1.04
New frequency peaks after attachment of physical TMD—experimental results	600 1150	0.524 1.005

Comparing the physical TMD system with its corresponding FE representation revealed a qualitatively comparable frequency redistribution. However, a significant difference between the frequency pairs of the physical and numerically optimized TMDs indicates that the physical TMD does not satisfy the optimum tuning criterion. The new frequency peaks observed in the physical TMD case show frequency redistribution and vibration attenuation. However, they do not quantitatively validate the chatter stability limit of the numerically optimized TMD model. Moreover, these machining runs were performed at a depth of cut of 0.5 mm, which falls well within the safe cutting zone for the numerically predicted limiting depth of cut of both TMDs. This means the operational dynamic behavior was observed under stable cutting conditions and therefore does not validate the chatter-onset criterion or the predicted enhancement in limiting depth of cut. Experimental validation of the predicted stability lobes would require chatter monitoring at various spindle speeds and depths of cut.

7. Practical Implications

The proposed methodology for an additively manufactured practical TMD for real-world applications has scope for potential applications in a wide range of areas like aerospace, automotive, medical devices and the energy sector.

- Deep hole boring applications for industries, requiring precision in defining internal features, such as engine components and hydraulic systems for aerospace, medi-

cal devices like surgical instruments and implants, fuel injection systems and engine blocks in automotive sector and turbine components and valve bodies in the energy sector.

- The proposed methodology could also be extended to other commercial large-scale machining operations like milling.
- The additive manufacturing approach could enable industrial expansion. This rapid-prototyping approach followed to fabricate optimized configurations of components or parts would significantly reduce development time and cost thus making custom-optimized TMDs economically and technically viable for smaller production units. Furthermore, the geometric freedom available through this methodology could be leveraged to build sophisticated damper configurations, leading to a higher performance ceiling.

8. Conclusions and Future Work

This study proposed and validated a hybrid DOE-FEA optimization model for chatter suppression in boring process with an additively manufactured passive tuned mass damper. The methodology integrated finite element forced vibration response analysis, analytical stability evaluation of chatter based on the Altintas frequency-domain criteria and RSM for constrained optimization of the absorber parameters under realistic manufacturing considerations. A key contribution of this work is the development of an externally mounted TDOF TMD additively manufactured using PLA as a practical and customizable passive vibration control solution for boring applications. The proposed design has flexibility in terms of implementation, manufacturability and retrofitting in existing boring setups, unlike the conventional internally integrated damping systems. The numerical analysis showed that the proposed optimization framework was able to draw attention to the influence of absorber position, stiffness and damping on chatter stability and provided information on an optimum absorber configuration. Comparative stability lobe analysis demonstrated the performance of the optimized TDOF TMD for chatter suppression was better than that of the conventional SDOF absorber, both in terms of limiting depth of cut and width of stable operating regions owing to the cumulative effect of absorber architecture, mass, stiffness and damping distribution and dynamic tuning. The experimental investigation using additively manufactured SDOF and TDOF TMD configuration served to demonstrate qualitative dynamic behaviour vibration attenuation and frequency redistribution of the dominant mode observed through time-domain acceleration response, power spectrum analysis and spectrogram. Consequently, considering the physical stiffness and mass parameters differed from those of the numerically optimized TMD, the experiments do not verify the predicted chatter stability limit. Furthermore, the machining runs performed at a single depth of cut within the predicted stable cutting zone meant that this experimental investigation could not be used to verify the predicted stability boundaries. The experimental investigation carried out as part of the present work should instead be considered as a demonstration of proof-of-concept of dynamic behaviour of the externally mounted additively manufactured TMD architecture. The approach presented in the current work is practically feasible and industrially viable to enhance the stability of boring operation, especially with the use of a slender boring bar, from a practical perspective. The externally mounted modular absorber concept is also flexible enough for tuning the system according to various machining configurations.

However, the present work encounters limitations in the form of constraints in considering more independent parameters as it would complicate the design space. The inability to consider nonlinearities by virtue of tool 3D geometric features due to the consideration of a simple lumped-system model on ANSYS Mechanical APDL limits its fidelity.

Furthermore, the limited reliability of numerical free and forced vibration analysis in comparison to a conventional experimental modal analysis raises questions on the credibility of the reported modal parameters. The use of a low degrees of freedom statistical DOE model tends to exaggerate the predictive power of the model owing to the possibility of overparameterization. On the fabrication side, limitations in leveraging the complete material properties of PLA due to untested thermal/fatigue behaviour of PLA imposed constraints on the tuneability of the additively manufactured TMDs. It is also accepted that the physical absorber fails to accommodate stiffness and damping values equivalent to the range of values considered in the numerical model. A limited experimental validation with only one machining condition directed towards validating the dynamic behaviour of the proposed numerical model (vibration attenuation, operational frequency redistribution and a comparison between the dynamic behaviour of SDOF and TDOF TMDs) fails to provide adequate reinforcement to the claims of the numerically optimized model. Moreover, the experimental validation performed for limited machining conditions does not accommodate the complete stability boundary aimed at validating the optimal parameters determined through the numerical optimization approach.

Future research directions may focus on extending the absorber design to higher order multi-degree-of-freedom; integrating machine learning based surrogate optimization to handle a multimodal nonlinear design space; and incorporating multi-objective optimization criteria which consider limiting depth of cut, lobe shape characteristics, and robustness against parameter uncertainty. The approach could also be extended into a global optimization framework to determine multiple possible optimum absorber configurations obeying the equal-trough stability criterion, further enhancing the impact of the current work. A comparison of the performance of SDOF and TDOF TMDs under similar independent parameter ranges would highlight the effect of the added degree of freedom towards chatter stability. Moreover, modal correlation of assembled boring bar-TMD system through experimental modal analysis and a comprehensive experimental validation of the predicted optimum limiting depth of cut through chatter onset tests over a range of spindle speed and increasing depth of cut values would harbor significant reproducibility to the proposed framework. The possibility of replacing the discrete spring element with a continuous structural element to accommodate higher stiffness requirements to match and experimentally validate the numerical model would add another dimension to the future scope of the present work.

Author Contributions: S.S. contributed to conceptualization, methodology, software development, investigation, data curation, formal analysis, visualization, and writing original draft preparation. S.C. contributed to methodology, software development, investigation, data curation, and visualization. K.P.J. contributed to methodology, software development, investigation, data curation, and visualization. J.P. contributed to methodology, validation, formal analysis, writing review and editing, supervision, resources, and funding acquisition. T.M. contributed to conceptualization, methodology, validation, formal analysis, writing review and editing, supervision, resources, and project administration. All authors have read and agreed to the published version of the manuscript.

Funding: The authors extend their acknowledgement to the financial support of the European Union under the REFRESH-Research Excellence for Region Sustainability and High-tech Industries project number CZ.10.03.01/00/22_003/0000048 via the Operational Programme Just Transition.

Data Availability Statement: The original contributions presented in this study are included in the article. Further inquiries can be directed at the corresponding authors.

Conflicts of Interest: The authors declare no conflicts of interest. The authors declare that they have no known competing financial interests or personal relationships that could have appeared to influence the work reported in this paper.

Abbreviations

The following abbreviations are used in this manuscript:

TMD	Tuned Mass Damper
SDOF	Single Degree of Freedom
TDOF	Two Degrees of Freedom
PLA	Polylactic Acid
RSM	Response surface methodology
ABS	Acrylonitrile Butadiene Styrene
FRF	Frequency Response Function
MR fluid	Magnetorheological fluid
FDM	Fused Deposition Modelling
CCD	Central Composite Design
ANOVA	Analysis of Variance
DOC	Depth of Cut
DOE	Design of Experiments
DOE-FEA	Design of Experiments–Finite Element Analysis

References

1. Çetindağ, H.A.; Oezkaya, E.; Çiçek, A.; Aslantas, K. Review of chatter control techniques in turning and boring. *Int. J. Adv. Manuf. Technol.* **2025**, *139*, 5363–5407. [CrossRef]
2. Li, S.; Yang, T.; Qin, X.; Li, H.; Liu, J.; Zhao, Q. Vibration control of boring bar in variable-parameter turning process with stiffness and damping adaptive TMD. *Int. J. Adv. Manuf. Technol.* **2025**, *139*, 5953–5967. [CrossRef]
3. Sun, H.-Y.; Jin, H.-Y.; Song, J.-X.; Han, Z.-Y.; Fu, H.-Y. A review of cutting chatter suppression methods. *Adv. Manuf.* **2025**, *14*, 211–243. [CrossRef]
4. Liu, Q.; Li, J.; Ma, J.; Gao, D.; Han, J.; Li, J. Structure design and vibration control of vibration reduction boring bar with variable damping. *Int. J. Adv. Manuf. Technol.* **2024**, *134*, 5301–5319. [CrossRef]
5. Sims, N.D. Vibration absorbers for chatter suppression: A new analytical tuning methodology. *J. Sound Vib.* **2007**, *301*, 592–607. [CrossRef]
6. Yang, Y.; Dai, W.; Liu, Q. Design and implementation of two-degree-of-freedom tuned mass damper in milling vibration mitigation. *J. Sound Vib.* **2015**, *335*, 78–88. [CrossRef]
7. Wang, M.; Qin, P.; Zan, T.; Gao, X.; Han, B.; Zhang, Y. Improving optimal chatter control of slender cutting tool through more accurate tuned mass damper modeling. *J. Sound Vib.* **2021**, *513*, 116393. [CrossRef]
8. Ma, W.; Yu, J.; Yang, Y.; Wang, Y. Optimization and Tuning of Passive Tuned Mass Damper Embedded in Milling Tool for Chatter Mitigation. *J. Manuf. Mater. Process.* **2021**, *5*, 2. [CrossRef]
9. Burattini, L.; Palmieri, M.; Landi, L. Design and Realization of a Mass Damper for a Die Cutting Machine. *Machines* **2025**, *13*, 1088. [CrossRef]
10. Burtscher, J.; Fleischer, J. Adaptive tuned mass damper with variable mass for chatter avoidance. *CIRP Ann.* **2017**, *66*, 397–400. [CrossRef]
11. Nakano, Y.; Kishi, T.; Takahara, H. Experimental Study on Application of Tuned Mass Dampers for Chatter in Turning of a Thin-Walled Cylinder. *Appl. Sci.* **2021**, *11*, 12070. [CrossRef]
12. Selvakumar, M.; Venugopal, P.R.; Velayudhan, G. Optimization of Tuned Mass Damper Location for Enhanced Chatter Suppression in Thin-wall Milling. *Stroj. Vestn.-J. Mech. Eng.* **2022**, *68*, 339–349. [CrossRef]
13. Mei, D.; Kong, T.; Shih, A.J.; Chen, Z. Magnetorheological fluid-controlled boring bar for chatter suppression. *J. Mater. Process. Technol.* **2009**, *209*, 1861–1870. [CrossRef]
14. Vishal Krishna, V.; Saravanamurugan, S.; Sanjeev Kishore, P.; Yedhu, K.J.; Iswar, G.K.; Shanmughasundaram, A. Vibration control in boring process using a constrained viscoelastic layer damper. *IOP Conf. Ser. Mater. Sci. Eng.* **2021**, *1059*, 012031. [CrossRef]
15. Guo, X.; Zhu, Y.; Luo, Z.; Cao, D.; Yang, J. Variable stiffness tuned particle dampers for vibration control of cantilever boring bars. *Appl. Math. Mech.* **2023**, *44*, 2163–2186. [CrossRef]
16. Zhang, H.; Song, J.; Zhao, J.; Ren, X.; Jiang, A.; Wang, B. Research Progress and Application of Vibration Suppression Technologies for Damped Boring Tools. *Machines* **2025**, *13*, 883. [CrossRef]
17. Hintze, W.; Hinrichs, M.; Rosenthal, O.; Schleinkofer, U.; Venturini, R. Model based design of tuned mass dampers for boring bars of small diameter. *Procedia CIRP* **2023**, *117*, 193–198. [CrossRef]

18. Li, L.; Yang, D.L.; Cui, Y.M. Optimization of machining performance in deep hole boring: A study on cutting tool vibration and dynamic vibration absorber design. *Adv. Prod. Eng. Manag.* **2023**, *18*, 371–380. [CrossRef]
19. Altintas, Y.; Lappin, D.; van Zyl, D.; Östling, D. Automatically tuned boring bar system. *CIRP Ann.* **2021**, *70*, 313–316. [CrossRef]
20. Biju, C.V.; Shunmugam, M.S. Performance of magnetorheological fluid based tunable frequency boring bar in chatter control. *Measurement* **2019**, *140*, 407–415. [CrossRef]
21. Hayati, S.; Shahrokhi, M.; Hedayati, A. Development of a frictionally damped boring bar for chatter suppression in boring process. *Int. J. Adv. Manuf. Technol.* **2021**, *113*, 2761–2778. [CrossRef]
22. Moradi, H.; Bakhtiari-Nejad, F.; Movahhedy, M.R. Tuneable vibration absorber design to suppress vibrations: An application in boring manufacturing process. *J. Sound Vib.* **2008**, *318*, 93–108. [CrossRef]
23. Rubio, L.; Loya, J.A.; Miguélez, M.H.; Fernández-Sáez, J. Optimization of passive vibration absorbers to reduce chatter in boring. *Mech. Syst. Signal Process.* **2013**, *41*, 691–704. [CrossRef]
24. Yang, G. State filtered disturbance rejection control. *Nonlinear Dyn.* **2025**, *113*, 6739–6755. [CrossRef]
25. Nasiri, K.; Moradi, H. Chatter suppression in nonlinear milling of a flexible plate-workpiece with attached piezoelectric actuators: Comparison of soft-actor-critic-based controller vs optimized type-2 fuzzy controller. *Mech. Syst. Signal Process.* **2025**, *224*, 112198. [CrossRef]
26. Yang, G.; Yao, J.; Ullah, N. Neuroadaptive control of saturated nonlinear systems with disturbance compensation. *ISA Trans.* **2022**, *122*, 49–62. [CrossRef] [PubMed]
27. Sundaram, S.; Puthenveetil, F.; Nair, V.S.; Krishnaswamy, R. The influence of material stiffness and damping on machining stability in boring tool–workpiece systems using finite element simulation to implement digital twin. *Int. J. Interact. Des. Manuf. IJIDeM* **2024**, *18*, 6765–6784. [CrossRef]
28. Betters, E.D.; West, J.; Noakes, M.; Nycz, A.; Smith, S.; Schmitz, T.L. Dynamic stiffness modification by internal features in additive manufacturing. *Precis. Eng.* **2020**, *66*, 125–134. [CrossRef]
29. Irska, I.; Kramek, G.; Miądlicki, K.; Dunaj, P.; Berczyński, S.; Piesowicz, E. Towards Highly Efficient, Additively Manufactured Passive Vibration Eliminators for Mechanical Systems. *Materials* **2023**, *16*, 1250. [CrossRef] [PubMed]
30. Jaradat, M.; Soliman, E.; Reda Taha, M. 3D-printed bio-inspired mechanically interlocked viscoelastic dampers for energy dissipation. *Mater. Des.* **2023**, *228*, 111826. [CrossRef]
31. Zu, R.; Chen, W.; Huang, Y.; Chen, Y.; Du, C.; Fan, Q.; Li, H.; Liu, H. Tailor-made 3D printing TPU/PLA composites for damping and energy absorption. *Mater. Des.* **2025**, *252*, 113752. [CrossRef]
32. Reichl, K.K.; Avci, O.; Inman, D.J. Temperature Dependent Damping in Additively Manufactured Polymer Structures. *J. Appl. Comput. Mech.* **2021**, *7*, 993–1008. [CrossRef]
33. Altintas, Y. *Manufacturing Automation: Metal Cutting Mechanics, Machine Tool Vibrations, and CNC Design*, 2nd ed.; Cambridge University Press: Cambridge, UK, 2012.
34. Demiryurek, S.G. Evaluation of dynamic properties in ABS and PLA thermoplastics across frequency ranges. *Sci. Rep.* **2025**, *15*, 42629. [CrossRef] [PubMed]
35. Rodríguez-Panes, A.; Claver, J.; Camacho, A.M. The influence of manufacturing parameters on the mechanical behaviour of PLA and ABS pieces manufactured by FDM: A comparative analysis. *Materials* **2018**, *11*, 1333. [CrossRef] [PubMed]
36. D'Andrea, D.; Risitano, G.; Raffaele, M.; Cucinotta, F.; Santonocito, D. Damage assessment of different FDM-processed materials adopting Infrared Thermography. *Fract. Struct. Integr.* **2022**, *16*, 75–90. [CrossRef]
37. Rădulescu, B.; Mihalache, A.M.; Hriţuc, A.; Rădulescu, M.; Slătineanu, L.; Munteanu, A.; Dodun, O.; Nagîţ, G. Thermal expansion of plastics used for 3D printing. *Polymers* **2022**, *14*, 3061. [CrossRef] [PubMed]
38. Schmitz, T.L.; Smith, K.S. *Machining dynamics: Frequency Response to Improved Productivity*; Springer: Cham, Switzerland, 2009.

Disclaimer/Publisher's Note: The statements, opinions and data contained in all publications are solely those of the individual author(s) and contributor(s) and not of MDPI and/or the editor(s). MDPI and/or the editor(s) disclaim responsibility for any injury to people or property resulting from any ideas, methods, instructions or products referred to in the content.